The noble gas geochemistry of natural CO2 gas reservoirs from the Colorado Plateau and Rocky Mountain provinces, USA

Cite As: Gilfillan, S, Ballentine, CJ, Holland, G, Blagburn, D, Lollar, BS, Stevens, S, Schoell, M & Cassidy, M 2008, 'The noble gas geochemistry of natural CO2 gas reservoirs from the Colorado Plateau and Rocky Mountain provinces, USA' *Geochimica et Cosmochimica Acta*, vol 72, no. 4, pp. 1174-1198.

DOI: 10.1016/j.gca.2007.10.009

The noble gas geochemistry of natural CO_2 gas reservoirs from the Colorado Plateau and Rocky Mountain provinces, USA

Stuart M.V. Gilfillan[1*], Chris J. Ballentine[1], Greg Holland[1], Dave Blagburn[1], Barbara Sherwood Lollar[2], Scott Stevens[3], Martin Schoell[4] and Martin Cassidy[5]

[1] School of Earth, Atmospheric and Environmental Sciences (SEAES), The University of Manchester, Oxford Road, Manchester, U.K. M13 9PL

[2] Department of Geology, University of Toronto, 22 Russell Street, Toronto, Ontario M5S 3B1, Canada

[3] Advanced Resources International, 4501 Fairfax Drive, Suite 910, Arlington, Virginia. 22203-1661

[4] Gas Consult International, 693 St. George Road, Danville. CA 94526

[5] Department of Geosciences, University of Houston, Houston, Texas. 77204-5503

*Author to whom correspondence should be addressed, now at:

School of Geosciences,
University of Edinburgh,
Grant Institute,
Kings Buildings,
West Mains Road,
Edinburgh, U.K.
EH9 3JW
E-mail: stuart.gilfillan@ed.ac.uk
Telephone: +44 (0) 131 650 7010
Fax: +44 (0) 131 668 3184

ABSTRACT

Identification of the source of CO_2 in natural reservoirs and development of physical models to account for the migration and interaction of this CO_2 with the groundwater is essential for developing a quantitative understanding of the long term storage potential of CO_2 in the subsurface. We present the results of 57 noble gas determinations in CO_2 rich fields (>82%) from three natural reservoirs to the east of the Colorado Plateau uplift province, USA (Bravo Dome, NM., Sheep Mountain, CO. and McCallum Dome, CO.), and from two reservoirs from within the uplift area (St Johns Dome, AZ., and McElmo Dome, CO.). We demonstrate that all fields have $CO_2/^3He$ ratios consistent with a dominantly magmatic source. The most recent volcanics in the province date from 8 – 10 ka and are associated with the Bravo Dome field. The oldest magmatic activity dates from 42 - 70 Ma and is associated with the McElmo Dome field, located in the tectonically stable centre of the Colorado Plateau: CO_2 can be stored within the subsurface on a millennia timescale.

The manner and extent of contact of the CO_2 phase with the groundwater system is a critical parameter in using these systems as natural analogues for geological storage of anthropogenic CO_2. We show that coherent fractionation of groundwater $^{20}Ne/^{36}Ar$ with crustal radiogenic noble gases (^4He, ^{21}Ne, ^{40}Ar) is explained by a two stage re-dissolution model: Stage 1: Magmatic CO_2 injection into the groundwater system strips dissolved air-derived noble gases (ASW) and accumulated crustal/radiogenic noble gas by CO_2/water phase partitioning. The CO_2 containing the groundwater stripped gases provides the first reservoir fluid charge. Subsequent charges of CO_2 provide no more ASW or crustal noble gases, and serve only to dilute the original ASW and crustal noble gas rich CO_2. Reservoir scale preservation of concentration gradients in ASW-derived noble gases thus provide CO_2 filling direction. This is seen in the Bravo Dome and St Johns Dome fields. Stage 2: The noble gases re-dissolve into any available gas stripped groundwater. This is modeled as a Rayleigh distillation process and enables us to quantify for each sample: 1) the volume of groundwater originally 'stripped' on reservoir filling; and 2) the volume of groundwater involved in subsequent interaction. The original water volume that is gas stripped varies from as low as 0.0005 cm^3 groundwater/cm^3 gas (STP) in one Bravo Dome sample, to 2.56 cm^3 groundwater/cm^3 gas (STP) in a St Johns Dome sample. Subsequent gas/groundwater

equilibration varies within all fields, each showing a remarkably similar range, from zero to ~100 cm^3 water/cm^3 gas (at reservoir pressure and temperature).

1. INTRODUCTION

Carbon dioxide (CO_2) has been identified as the most important compound currently affecting the stability of the Earth's climate and represents 62.5% of globally generated greenhouse gases (International Panel on Climate Change, 1996; 2001; 2007). Geologic storage of anthropogenic CO_2 in depleted oil and gas reservoirs is one of the key options for short-term control of CO_2 emissions. However, CO_2 is a reactive gas that has significantly more influence upon the host rocks and their formation waters than petroleum fluids (Baines and Worden, 2004). In order for this technology to be safely implemented the long term consequence of injecting CO_2 into the subsurface must be quantified.

Natural subsurface CO_2 accumulations have existed on geological timescales and provide key analogues that inform us about the feasibility of long term storage of anthropogenic CO_2 (e.g. Baines and Worden, 2004; Haszeldine et al., 2005). Despite the amount of information available from these sites, in many natural CO_2 reservoirs the source of the CO_2 and basin scale processes that act on them are poorly understood. This is partially due to the multiple origins of CO_2 in natural gases. These include methanogenesis, oil field biodegradation, kerogen decarboxyilation, hydrocarbon oxidation, decarbonation of marine carbonates and degassing of magmatic bodies (Jenden et al., 1993; Wycherley et al., 1999). $\delta^{13}C(CO_2)$ can be used to distinguish between some of these different sources. However, the $\delta^{13}C(CO_2)$ of natural gas fields containing high CO_2 concentrations (>70% CO_2) almost always lies in the overlapping range between magmatic degassing and carbonate breakdown, and these different sources cannot be readily distinguished. In addition, because of the high CO_2 solubility in water and CO_2 reactivity, the extent of interaction of the CO_2 phase with the groundwater is a critical parameter in quantifying CO_2 sinks. The groundwater systems associated with CO_2 gas deposits are often similar to those of oil and gas field brines and there are few techniques available to quantify regional groundwater movement through age/residence time determination or the groundwater volumes that have interacted with the trapped reservoir phase.

Noble gas isotopic and abundance measurements can be used to constrain CO_2 origins and subsurface interaction with the groundwater system. This is because noble gases from the terrestrial atmosphere, dissolved in groundwater, can be distinguished isotopically from those from the mantle that contain a primordial signature, and those produced by the radiogenic decay of U, Th and K within the crust. When combined with the distinct elemental abundance patterns of the different sources, it is possible to resolve the relative noble gas input from each source to any crustal fluid. This allows the extent of crustal, mantle and atmospheric contributions to the fluid to be constrained (e.g. Ballentine et al., 2002). Additionally, noble gases can be used to constrain natural gas associated water residence times (Zhou and et al., 2005) and quantify the degree of interaction a crustal fluid has had with the groundwater system (Ballentine et al., 1991; Pinti and Marty, 1995; Ballentine et al., 1996; Torgersen and Kennedy, 1999; Ballentine and Sherwood Lollar 2002; Zhou et al., 2005).

Whilst primordial noble gas isotopes have been studied in CO_2-rich well gases since 1961 (e.g. Zartman et al., 1961; Phinney et al., 1978; Caffee et al., 1999; Ballentine et al., 2005; Holland and Ballentine 2006), no systematic study using a full noble gas data set to investigate CO_2 origin and quantify its interaction with the groundwater system subsurface has yet been undertaken. Here we present a He, Ne, Ar, Kr and Xe isotopic study of the CO_2 from five separate producing gas fields located throughout the Colorado Plateau and Rocky Mountain provinces. In this paper we show how measured $CO_2/^3He$ ratios enable us to determine the CO_2 source in each system. We then use the noble gases to identify the subsurface processes acting on the CO_2 and develop a quantitative model of gas and groundwater interaction.

2. THE COLORADO PLATEAU AND ROCKY MOUNTAIN NATURAL CO_2 RESERVOIRS

The Colorado Plateau is a massive, high-standing tectonic block located in the south western US, centred on the Four Corners of the states of Colorado, New Mexico, Utah and Arizona (Fig. 1). It is abruptly flanked to the east by the majestic Rocky Mountains, the result of at least 2 km of uplift during the Laramide Orogeny and later Cenozoic uplifts (Baars, 2000). The bulk of magmatic activity on the Colorado Plateau occurred in the Late Cenozoic, along the transitional south western margin (primary between 5-15 Ma) and the northwest southeast trending Rio Grande Rift (0 - 5 Ma) (Fitton et al., 1991). This has coincided with the most-recent and best constrained uplift event at the Plateau's southwest margin between 6 Ma and

1 Ma (Parsons and McCarthy, 1995). The province contains at least nine producing or abandoned gas fields that contain up to 2800 billion m^3 of natural CO_2 (Allis et al., 2001). At the present time the authors are aware of five fields that are commercially producing CO_2, primarily for Enhanced Oil Recovery (EOR) and industrial use, and one field which is currently under development. The majority of the fields are fault bounded anticlines which have four way anticlinal closure or a fault seal along one of the field margins (Shipton et al., 2004).

We focus on the following reservoirs: McCallum Dome, (Jackson Co, CO); Sheep Mountain, (Huerfano County, CO); Bravo Dome, (Harding County, NM); McElmo Dome and the related field Doe Canyon, (Montezuma County, CO) and St Johns Dome (Apache County, AZ) (Fig. 1.). All of these sites contain extremely high CO_2 concentrations, averaging 95-99% CO_2, 1-4% N_2, 0.1-1% He and other trace gases (Allis et al., 2001). We provide detail of the individual geological setting and in particular the relationship of all of these fields to nearby volcanic features associated with the Colorado Plateau uplift event in the Appendix.

3. SAMPLE COLLECTION AND ANALYTICAL TECHNIQUES

Samples from the gas fields were collected directly from producing wellheads that tap the natural gas reservoirs. Sample localities were chosen on site to provide a wide range of depth and spatial distribution across the fields. Samples were collected via the conventional ¾-inch National Pipe Thread (NPT) sample port of the well head using two field-sampling techniques.

At McElmo Dome the gas was allowed to flow through a 60 cm length of 10 mm diameter, internally polished refrigeration grade copper tubing before being sealed at either end at close to atmospheric pressure following the technique described by Ballentine and Sherwood Lollar (2002). At St. John's Dome, McCallum Dome, Sheep Mountain and Bravo Dome samples were collected in Swagelok® 300 ml stainless steel sampling cylinders fitted at both ends with two high-pressure valves. All cylinders were baked at 150 ºC under vacuum before being shipped to the field. The cylinders were attached directly to the sampling port of the wellhead prior to the gas undergoing any form of commercial processing. A 20 cm length of high pressure hosing was attached to the other end of the cylinder as an exhaust to prevent turbulent back mixing. The cylinders were flushed through with gas from the wellhead for 5 minutes before the outer valve was shut and the cylinder equilibrated at wellhead pressure, which ranged from 1400 – 3500 Pa. The cylinder valve closest to the well head was then shut and the gas vented by opening the outer cylinder valve. This valve was closed before complete positive pressure was lost. This purge procedure was repeated 5 more times before all valves were closed sequentially from the outer valve to the valve closest to the sampling port.

Noble gas abundance and isotopes for all samples except those from Bravo Dome (documented in Ballentine et al., (2005)) were determined at the University of Manchester using an all metal purification line and a MAP 215 mass spectrometer. Sub-samples for stable isotope determination are reported elsewhere. Aliquots of the samples were expanded into a calibrated volume of 69.37 cm^3 containing a Baratron® at known temperature. This volume only was expanded onto a Ti sponge furnace, preheated to 1173 K, and then cooled to room temperature over 15 minutes. Subsequently, the sample was equilibrated with a Zr-Al SAES® getter heated to 523 K, to remove most of the active gases, and then equilibrated with charcoal held at 77.3 K to trap the Ar, Kr and Xe, leaving only He and Ne free in the vacuum line. The He and Ne was then expanded into an additional calibrated storage volume of 718 cm^3 fitted with a 1 cm^3 pipette. The volume of CO_2 administered for analysis varied from 3 cm^3 to 38 cm^3 (STP) depending on the concentration of noble gases within the sample.

For He analysis a 1 cm^3 aliquot from the storage volume was expanded into the UHV mass spectrometer extraction line, where the sample was further cleaned on a SAES® GP50 getter at 523 K and a SAES® GP50 getter at 293 K before admission to the mass spectrometer for analysis. A second aliquot (~35 cm^3) was taken from the storage volume, purified on both the GP50 and NP10 getters, and the Ne separated from He on a cryogenic activated charcoal trap at 38 K. The Ne was subsequently expanded onto a charcoal trap at 77.3 K to remove any residual ^{40}Ar and reduce interference on the ^{20}Ne measurements, and inlet into the mass spectrometer for analysis. Following evacuation of the mass spectrometer and the storage volume after Ne analysis the charcoal trap containing the Ar, Kr and Xe was heated to ~253 K and the gas expanded into the storage volume. A 35 cm^3 aliquot was expanded onto the GP50 and NP10 getters for further purification and then expanded into the mass spectrometer for Ar and Kr determination. The remaining gas in the storage bottle was expanded onto an activated charcoal trap held at 163 K, quantitatively trapping the Xe, some Kr and allowing the Ar to be pumped away. On warming the charcoal trap to ~253 K, the Xe was released and then inlet into the mass spectrometer for determination.

Mass spectrometer sensitivity and mass discrimination were calibrated by comparison to standards prepared from known volumes of dry air. Full procedural blanks were measured before, during and after the analysis program. Blanks were indistinguishable from atmosphere isotopic compositions. Blank levels were negligible compared to original sample size for all isotopes except ^{20}Ne, which was typically <1%, with the exception of two of the Sheep Mountain samples (2-10-O and 3-23-D), and those of McElmo Dome. Blank correction in the McElmo Dome samples varied from 0.27% to a maximum of 8.5% in two cases. During isotope and abundance analysis, appropriate mass peaks were monitored to correct for interferences caused by the doubly charged ions of $^{40}Ar^{2+}$ and $^{44}CO_2^{2++}$. These were found to be negligible in all cases. Quoted errors are at the 1σ level of confidence and

include statistical analytical error, air standard reproducibility, the expansion volume uncertainty and mass spectrometer sensitivity stability.

4. RESULTS

A total of fifty seven deep well gas samples from the five gas reservoirs were collected. Table 1 documents the sample location, well depth and the results of noble gas isotopic composition measurements ($^{3}He/^{4}He$, $^{20}Ne/^{22}Ne$, $^{21}Ne/^{22}Ne$ and $^{40}Ar/^{36}Ar$). Table 2 outlines the major component abundance (CO_2, N_2, and CH_4) and noble gas abundance measurements (^{4}He, ^{20}Ne, ^{40}Ar, ^{84}Kr). For several Bravo Dome, Sheep Mountain and four McElmo Dome samples ^{130}Xe and $^{130}Xe/^{136}Xe$ was also determined.

4.1. Major gas species

CO_2 concentrations in all fields typically range from 92-99% with the exception of two samples from the St. John's Dome field and the single sample from Doe Canyon (near McElmo Dome). The remaining gas is dominated by N_2, CH_4, trace C_2H_6 and noble gases. Within both St Johns Dome and McElmo Dome fields, the only fields with individual sample gas composition measurements available, there is a positive correlation between the N_2 concentration and He concentration (Fig. 2). In the St. John's Dome this correlates to an increase in depth and proximity to the gas/groundwater contact within the field. The correlation of N_2 with He is similar to trends observed in the Hugoton-Panhandle giant gas field ascribed to accumulation of metamorphic N_2 and crustal ^{4}He in the regional groundwater and subsequent focussing though degassing (Ballentine and Sherwood Lollar, 2002).

4.2. $CO_2/^{3}He$ ratios and CO_2 origins

Figure 3 shows $CO_2/^{3}He$ ratios plotted against CO_2 concentration for all of the CO_2 gas fields. All of the samples from the gas fields have $CO_2/^{3}He$ ratios within or below the MORB range of 1×10^{9} to 1×10^{10} (Marty and Jambon, 1987). This is quite distinct from the higher $CO_2/^{3}He$ values predicted for near ^{3}He-free carbonates (Sherwood Lollar et al., 1997; Ballentine et al., 2001). The origin of the CO_2 in all fields, with the exception of the well studied Bravo Dome, has previously been thought to be derived from the thermal breakdown of carbonates. Our new results conclusively show that a significant proportion of the CO_2, if not all, is magmatic in origin. Whilst we believe the CO_2 to be predominantly mantle derived, and indeed all of the

fields are proximal to Late Cenozoic volcanism (Appendix), most CO_2 accumulations are multi-sourced (Baines and Worden, 2004). We cannot therefore rule out the addition of some crustal derived CO_2 to the reservoirs, particularly the single sample from McCallum Dome and several of the McElmo Dome samples which exhibit the highest well gas $CO_2/^3He$ ratios. The $CO_2/^3He$ ratios that are significantly lower than the MORB range in the St. John's Dome and Doe Canyon fields can only be ascribed to CO_2 loss or fractionation relative to ^3He subsequent to magmatic degassing (Sherwood Lollar et al., 1997).

4.3. Noble gases

4.3.1. Helium

Measured $^4He/^{20}Ne$ ratios in all fields are significantly above the air ratio of 0.032, showing that atmospheric He contributions to all samples are negligible. $^3He/^4He$ ratios therefore represent a mixture of crustal-radiogenic and mantle-derived helium (Fig. 4.).

The highest $^3He/^4He$ values are from the Bravo Dome field which shows a coherent variation from 3.78 to 0.764 R_a (where R_a is the atmospheric ratio) and increasing ^4He from west to east across the field towards the gas/groundwater contact (Ballentine et al., 2005). A similar pattern is seen in the McCallum field (0.354 to 0.448 R_a) where the North McCallum field shows a clear increase in ^4He concentration and a correlated reduction in the $^3He/^4He$ ratio. This pattern contrasts with St. John's Dome (0.394 to 0.455 R_a). $^3He/^4He$ ratios increase across the St Johns field toward the gas/groundwater contact, the increase in $^3He/^4He$ corresponds with a significant increase in ^4He concentration. $^3He/^4He$ ratios from within the Sheep Mountain (0.916 up to 1.06 R_a) and McElmo Dome (0.125 to 0.173 R_a) field show no spatial coherence indicating that either the crustal and mantle He components are well mixed before input into the gas field or have been homogenized within the reservoir subsequent to filling. The single sample from Doe Canyon has a significantly lower and more crustal radiogenic ratio of 0.065 R_a and correspondingly higher ^4He.

4.3.2. Neon

Within Bravo and St. Johns Dome there is a clear and coherent correlation between increasing ^{20}Ne concentrations and increased proximity to the Gas/Water contact. A similar trend can be seen in the bulk of the McCallum and Bravo Dome fields although it is masked

by several outlying data points. No such trend exists within the Sheep Mountain dataset implying that the Ne systematics are more complex than those of the other fields.

Figure 5 documents the $^{20}Ne/^{22}Ne$ and $^{21}Ne/^{22}Ne$ measured from all samples in the study. Three distinct trends can be identified using the Ne isotope data. The Bravo Dome field is the only system to exhibit mixing between a pre-mixed crust/air component and the mantle component. Sheep Mountain, St. John's and McCallum Domes illustrate a contrasting relationship between a pre-mixed crust/mantle component and air. McElmo Dome clearly contains the greatest contribution of crustal radiogenic components, which is reflected by the high $^{21}Ne/^{22}Ne$ ratios observed within the field but, unlike the other fields, shows no coherent mixing trend.

Uniquely amongst the noble gases, the contribution of atmospheric, mantle and crustal Ne components can be unambiguously resolved from the Ne isotopes alone (Ballentine, 1997). This is because the air, mantle and crustal end-member isotopic compositions are different and well defined ($^{20}Ne/^{22}Ne_{air}$ = 9.80, $^{21}Ne/^{22}Ne_{air}$ = 0.029, $^{20}Ne/^{22}Ne_{mntl}$ = 12.5, $^{21}Ne/^{22}Ne_{mntl}$ = 0.06, $^{20}Ne/^{22}Ne_{crust}$ = 0.30, $^{21}Ne/^{22}Ne_{crust}$ = 0.52 (Ballentine et al., 2002; Ballentine et al., 2005)). The range of calculated average $^{4}He/^{21}Ne_{crust}$ values of 2.89 x 10^7 to 5.08 x 10^7 within all of the fields are higher than both the measured average crust value of 1.71 x 10^7 and theoretical estimates of between 2.02 – 2.64 x 10^7 (Ballentine and Burnard, 2002). This is consistent with release from a shallow, low temperature regime (Ballentine et al., 1994; Ballentine and Sherwood Lollar 2002).

4.3.3. Argon

In all of the reservoirs bar Sheep Mountain ^{40}Ar correlates directly with ^{4}He and ^{20}Ne. A similar relationship exists between ^{36}Ar and ^{20}Ne within all the reservoirs and is particularly strong within Bravo, McCallum and St. Johns Dome. As with ^{20}Ne, ^{36}Ar increases with proximity to the Gas/Groundwater contact.

Measured $^{40}Ar/^{36}Ar$ ratios from all of the reservoirs are considerably above the air value of 295.5, as a result of a resolvable excess of ^{40}Ar ($^{40}Ar^*$) (Fig. 4). Helium isotopes indicate both mantle and crustal contributions to the noble gases, the $^{40}Ar^*$ is therefore a mixture of mantle and crustal-derived ^{40}Ar. In the case of Bravo Dome, $^{40}Ar^*/^{4}He$ correlates with $^{3}He/^{4}He$ isotope variation with a correlation coefficient of 0.993 (Ballentine et al., 2005). Extrapolating

to $^{3}He/^{4}He_{crust}$ = 1 x 10^{-8} (Ballentine and Burnard 2002) resolves $^{4}He/^{40}Ar_{crust}$ = 22.0. This is significantly above average crustal production of $^{4}He/^{40}Ar_{crust}$ = 5 and is consistent with the resolved $^{4}He/^{21}Ne_{crust}$ discussed above, indicating a thermal regime controlling the release of crustal radiogenic light noble gases in preference to heavier noble gases (Ballentine et al., 1994; Ballentine and Sherwood Lollar 2002). The mantle derived $^{4}He/^{40}Ar$ relationships at Bravo Dome are discussed elsewhere (Ballentine et al., 2005; Holland and Ballentine 2006). Within the other reservoirs, without significant $^{3}He/^{4}He$ variation, contributions to $^{40}Ar^{*}$ from both the mantle and crust cannot be simply resolved and the $^{40}Ar^{*}$ must be considered as a mix of the crustal and mantle components ($^{40}Ar_{crust+mantle}$).

$^{38}Ar/^{36}Ar$ values in all measured samples are indistinguishable from the atmospheric ratio. While the Bravo Dome samples are not reported here, a recent analysis of a second suite of samples are similarly indistinguishable from the air value suggesting that at the level of analytical precision no kinetic fractionation of Ar isotopes due to commercial production (e.g. Zhou et al., 2005) or significant radiogenic ^{36}Ar or ^{38}Ar contributions are resolvable.

4.3.4. Krypton, Xenon groundwater noble gas components

^{84}Kr in all fields correlate with ^{36}Ar and also with ^{20}Ne within Bravo, McCallum and St. Johns Domes. In both St. Johns and Bravo Domes there is a clear and coherent increase in ^{84}Kr on moving towards the gas/groundwater contact confirming that the majority of the ^{84}Kr is derived from the dissolved air component within the groundwater. ^{130}Xe within Bravo Dome exhibits a similar increase as observed in ^{20}Ne, ^{36}Ar and ^{84}Kr on moving eastwards towards the gas/water contact.

^{20}Ne and ^{36}Ar within crustal fluids are dominantly derived from the atmosphere dissolved in groundwater at recharge (Ballentine et al., 2002). Nevertheless, in these mantle-derived CO_2 fluids mantle and crustal ^{20}Ne and to a lesser extent ^{36}Ar may be present. Using the Ne isotope resolution technique outlined by Ballentine (1997) the atmospheric contribution to ^{20}Ne for each sample can be resolved. Within Bravo Dome a plot of $I/^{22}Ne$ vs $^{20}Ne/^{22}Ne$ vs $^{21}Ne/^{22}Ne$, where I is any noble gas isotope, defines a plane and enables the end member contribution to each noble gas isotope to be calculated and allows us to uniquely determine the $^{36}Ar_{(atm)}$ for each Bravo Dome sample. For this reason we use Bravo Dome as our reference system. Within the other fields the more limited spread of data does not make this

possible. Using the Ne isotopes we calculate the maximum ^{20}Ne mantle contribution to these fields is ~10%. This is small compared to the range of observed $^{20}Ne/^{36}Ar$ and we make the simplifying assumption that ^{20}Ne and ^{36}Ar is entirely groundwater-derived. Observed (mantle-corrected in the case of Bravo Dome) $^{20}Ne/^{36}Ar$ ratios are compiled in Table 3.

Bravo Dome $^{20}Ne/^{36}Ar_{(atm)}$ values range between 0.152 and 0.430 and compare with a reference air saturated water (ASW) value of 0.152. ASW is defined here as groundwater equilibrated with air at 10°C at an altitude of 2000 m and containing a 10% Ne excess air component. McElmo Dome samples show $^{20}Ne/^{36}Ar$ that ranges from below ASW at 0.061, to 0.389, similar to the upper limit of Bravo Dome. McCallum Dome $^{20}Ne/^{36}Ar$ ratios range from 0.312 up to 0.462, again similar to the Bravo Dome upper limit, while St Johns Dome samples range from 0.136 to 0.219, close to ASW. In contrast all Sheep Mountain samples are strongly fractionated relative to ASW. The majority of Sheep Mountain samples have $^{20}Ne/^{36}Ar$ ratios in the range of 0.530 to 1.31. However, four samples show $^{20}Ne/^{36}Ar$ values ranging from 2.01 to 3.08. Similar extreme values have been observed before in natural gases with $^{20}Ne/^{36}Ar_{(atm)}$ values up to 1.4 in CO_2-N_2 rich gases in the Indus Basin (Battani et al., 2000) and up to $^{20}Ne/^{36}Ar_{(atm)}$ of 4.9 in dry biogenic methane gases in the Macuspana basin, Mexico (Prinzhofer et al., 2000). The mechanisms that can account for the fractionation of $^{20}Ne/^{36}Ar$ in the gas phase from ASW are discussed in section 5.1.

Similar to ^{36}Ar, ^{84}Kr and ^{130}Xe in Bravo Dome samples can also be corrected for non-atmosphere (mantle) contributions using the Ne isotope system to define the $^{84}Kr/^{36}Ar_{mntl}$ and $^{130}Xe/^{36}Ar_{mntl}$ ratios (0.051 and 0.001045, respectively). ^{84}Kr and ^{130}Xe in all other gas fields are assumed to be dominantly atmospheric in origin. $^{84}Kr/^{36}Ar$ vs $^{20}Ne/^{36}Ar$ and $^{84}Kr/^{36}Ar$ vs $^{130}Xe/^{36}Ar$ is shown in Fig. 6a and 6b respectively. Mantle corrected $^{84}Kr/^{36}Ar$ ratios in Bravo Dome range from 0.013 to 0.026 compared with the ASW value of 0.045. A wider range in $^{84}Kr/^{36}Ar$ is observed in St. John's Dome, McElmo Dome and McCallum Dome with $^{84}Kr/^{36}Ar$ ratios varying from 0.021 to 0.072 over a relatively narrow $^{20}Ne/^{36}Ar$ range. In contrast, with the exception of a few samples, the majority of Sheep Mountain samples show only a small range in $^{84}Kr/^{36}Ar$ ratios, with the samples showing the most $^{20}Ne/^{36}Ar$ fractionation having $^{84}Kr/^{36}Ar$ ratios similar to the air value (0.020) (Fig. 6a). Within the McElmo Dome and Sheep Mountain fields there is a clear correlation between increasing $^{84}Kr/^{36}Ar$ and increasing

$^{130}Xe/^{36}Ar$ (Fig. 6b). Mantle corrected $^{130}Xe/^{36}Ar$ ratios from Bravo Dome exhibit a similarly narrow range to that observed in the $^{84}Kr/^{36}Ar$ (Fig. 6b).

4.3.5 Fractionation of groundwater and crustal-derived noble gases

The fractionation observed in the $^{20}Ne/^{36}Ar$ ratios within Bravo Dome and McCallum Dome correlates to some fractionation of the $^{4}He/^{40}Ar_{(crust+mantle)}$, and to a lesser degree the $^{4}He/^{21}Ne_{(crust+mantle)}$ ratios. Within Bravo Dome $^{4}He/^{40}Ar_{(crust+mantle)}$ ratios range from 1.64 to 6.79, a fourfold increase, whereas the $^{4}He/^{21}Ne_{(crust+mantle)}$ ratios double, from 8.90×10^{7} to 2.46×10^{7}. $^{4}He/^{40}Ar_{(crust+mantle)}$ values from McCallum Dome more than double from an initial value of 2.66 to 5.90, with $^{4}He/^{21}Ne_{(crust+mantle)}$ ratios only increasing from 2.24×10^{7} to 3.83×10^{7}. As the degree of $^{4}He/^{21}Ne_{(crust+mantle)}$ fractionation is less than that of $^{4}He/^{40}Ar_{(crust+mantle)}$ these fractionation trends are consistent with a solubility controlled gas/groundwater phase partition process (e.g. Ballentine et al. 1991). Coherent fractionation of the groundwater-derived and crustal radiogenic noble gases indicates that these differently sourced noble gases are premixed prior to the fractionation event, probably in the groundwater. In contrast, the extreme fractionation of the $^{20}Ne/^{36}Ar_{(atm)}$ ratios in the Sheep Mountain field does not correlate with any fractionation of the $^{4}He/^{40}Ar_{(crust+mantle)}$ or $^{4}He/^{21}Ne_{(crust+mantle)}$ ratios. Whilst $^{20}Ne/^{36}Ar$ fractionation in St. Johns Dome is small (0.125 to 0.170) there is nevertheless a clear correlation between the increase in $^{20}Ne/^{36}Ar$ and an increase in both $^{4}He/^{40}Ar$ and $^{4}He/^{21}Ne$ on moving towards the Gas/Groundwater contact. Observed McElmo Dome $^{20}Ne/^{36}Ar$ values are the only ones to significantly fall below the nominal ASW value of 0.152, by as much as 30%. Whilst there are also several $^{20}Ne/^{36}Ar$ values which are significantly above the ASW value of 0.152 no clear relationship between this fractionation and either $^{4}He/^{21}Ne$ or $^{4}He/^{40}Ar$ exists within the field. This could be because the fractionation processes which have been acting in the other reservoirs did not occur in this field or the groundwater system has been perturbed destroying any pre-existing correlations.

5. QUANTIFYING GAS/WATER VOLUMES

In the simplest case, equilibration of a large gas/water volume ratio in the subsurface will cause near quantitative degassing of the groundwater and result in a gas phase that has the groundwater, ASW, noble gas isotopic and elemental composition. As the subsurface gas/water volume ratio decreases the least soluble gases will tend to be enriched in the gas

phase until $V_{gas}/V_{water} \rightarrow 0$ when the limit of the enrichment is controlled by the relative solubility of the respective gases. For example, the maximum enrichment of the Ne relative to Ar in the gas phase though phase equilibrium degassing is K_{Ne}/K_{Ar} where K_{Ne} and K_{Ar} are the respective Henry's constants for Ne and Ar (e.g. Ballentine et al., 1991; 2002). K_{Ne} and K_{Ar} are given for average field conditions in Table 4 and predict a maximum enrichment of Ne relative to Ar from ASW values by a factor of ~2.

The $^{20}Ne/^{36}Ar$ in both Bravo and McElmo Dome CO_2 gases extend from groundwater elemental ratios to fractionated values that cannot be accounted for by simple equilibration between the CO_2 and groundwater phases. The preservation in some samples of ASW elemental ratios in these fields and the near ASW ratios in the St Johns Dome samples suggests that some degree of 'gas stripping' of the groundwater noble gas composition may be a common feature of these systems. Coherent fractionation of the crustal radiogenic noble gases, where fractionation has occurred, points to systems that are well mixed prior to the fractionating process. The fractionating process is therefore subsequent to the ASW gas stripping.

In contrast there is no overlap of the $^{20}Ne/^{36}Ar$ in the Sheep Mountain samples with the groundwater value, this system shows extreme $^{20}Ne/^{36}Ar$ fractionation and no coherence with the crustal radiogenic gases. While we make the simplifying assumption that the process of $^{20}Ne/^{36}Ar$ fractionation in the Sheep mountain CO_2 field is the same as that in the other gas fields, it is clear that Sheep Mountain is more complex: interaction between the CO_2 and a phase containing crustal radiogenic gases has occurred subsequent to the $^{20}Ne/^{36}Ar$ fractionating event. It is nevertheless, only by considering all systems that we can start to identify the common processes, and in particular the role of groundwater, in these critical analogues for CO_2 storage.

5.1. Fractionation of $^{20}Ne/^{36}Ar$ (and $^{84}Kr/^{36}Ar$, $^{130}Xe/^{36}Ar$)

We now consider the different processes that have the potential to fractionate $^{20}Ne/^{36}Ar$ (and $^{84}Kr/^{36}Ar$, $^{130}Xe/^{36}Ar$) beyond the limit imposed by simple gas/water phase equilibrium. As Ar, relative to Ne, is more soluble in oil than water, equilibration of the groundwater with an oil phase could increase the $^{20}Ne/^{36}Ar$ in the water phase (Bosch and Mazor 1988). Subsequent groundwater/CO_2 phase equilibration could then produce higher $^{20}Ne/^{36}Ar$ in the CO_2 gas

phase. However, with the exception of Sheep Mountain which is located near to a recent hydrocarbon gas discovery (Worrall, 2004) and McCallum Dome which is part of an actively producing oil field, there is no evidence of significant oil phase components in any of the reservoirs (Appendix). In the Indus Basin, where the high $^{20}Ne/^{36}Ar$ ratios have been attributed to oil involvement, there is a correlation between $^{20}Ne/^{36}Ar$ and $1/^{36}Ar$ ratios (Battani et al., 2000). There is no such correlation in the CO_2 gas fields of this study.

Similarly, $^{84}Kr/^{36}Ar$ and $^{130}Xe/^{36}Ar$ in excess of groundwater values (Fig. 6) may be caused by the release of atmosphere-derived Xe and Kr that is adsorbed and trapped in organic-rich sediments. $^{130}Xe/^{36}Ar$ enrichment factors up to ~200 relative to water in equilibrium with air have been observed (Fanale and Cannon, 1971; Kennedy et al., 1990; Torgersen and Kennedy, 1999; Kennedy et al., 2002; Torgersen et al., 2004). Direct evidence that Kr and Xe excesses survive sedimentary consolidation and low degrees of thermal alteration is documented in Kr and Xe excesses observed in gas released by the biogenic breakdown of coal (Zhou et al., 2005). However, whilst we cannot rule out this mechanism altogether, we discount organic-sediment derived Kr and Xe for the same reason that we discount oil-involvement in all reservoirs (except McCallum Dome and Sheep Mountain) as there is no organic-rich source rock.

The second mechanism we consider is non-equilibrium diffusion. Atmosphere-derived Ne, Kr and Xe excesses have been reported in secondary silica phases, volcanic glasses, tektites, and in MORB and OIB basalts (Matsubara and Matsuda, 1995; Matsuda et al., 1989; Pinti et al., 1999). Torgersen et al., (2004) have proposed that variable enrichments of noble gases can be accounted for by incomplete emptying followed by partial filling of lithic grains and half spaces, similar to the mechanism proposed by Pinti et al., 1999 for air diffusion into fresh pumice. Pinti et al., (*op cit*) further demonstrate that both elemental and isotopic compositions show clear mass dependent fractionation both between the elemental ratios and isotopic compositions of Ne and Ar. While the significant mantle and crustal Ne contributions makes subtle isotopic fractionation in Ne hard to identify, we observe no significant mass related fractionation in either the $^{38}Ar/^{36}Ar$ ratios or elemental abundance patterns and discount this as a significant fractionation mechanism for these reservoirs. We further note that in other gas reservoirs where mass dependant fractionation of the groundwater gases

has been observed in the $^{20}Ne/^{22}Ne$ and $^{38}Ar/^{36}Ar$ isotopic ratios, the dominant elemental fractionation is solubility controlled (Zhou et al., 2005).

In principle multiple stages of exsolution and dissolution can increase the solubility fractionation limit (Zartman et al., 1961). In this case a gas phase exsolved from the water with a low Gas/Water volume ratio will have an elevated $^{20}Ne/^{36}Ar$ ratio. This could be re-dissolved into a smaller volume of water by a change in physical conditions such as a pressure increase, a decrease in temperature and salinity, or mixing with unsaturated (with respect to the gas phase) water. This creates a local increase in both the groundwater noble gas concentration and the magnitude of noble gas fractionation in solution. Subsequent formation of a gas phase in equilibrium with the now modified groundwater could show a fractionation significantly in excess of that predicted by the single stage equilibrium model. To achieve this, the pressure/temperature conditions must fluctuate and the resulting fractionated gas phase volume is very small compared to the fluid/water volume required to produce any significant fractionation (Ballentine et al., 2002) and we discount this as a viable gas field scale mechanism.

We now consider a partial re-dissolution model (Fig. 9). This is a two stage process. Stage one is the complete degassing of the groundwater noble gases into the gas phase. Stage two is partial re-equilibration (closed system) or Rayleigh fractionation (open system) caused by re-dissolution of the noble gases from the gas phase into a noble gas stripped groundwater (possibly caused regionally by stage 1).

5.1.1. Bravo Dome

Average reservoir conditions and Henry's constants are given in Table 4. Neither closed system batch fractionation nor open system Rayleigh degassing models of gas exsolving from an ASW groundwater phase can account for the observed maximum fractionation (Fig. 7). The high $^{20}Ne/^{36}Ar_{(atm)}$ and low $^{84}Kr/^{36}Ar_{(atm)}$ values can however, be explained by the re-dissolution model. Since CO_2 is a significantly better solvent than water (King et al., 1992), noble gases will preferentially partition into the CO_2 in the subsurface. In the case of the Bravo Dome field we argue that gas stripping of the groundwater system associated with the gas field occurs through the injection and movement of magmatic CO_2 through the groundwater during an initial reservoir filling stage. The ^{20}Ne concentration in the gas phase,

orders of magnitude lower than that predicted by groundwater degassing (Fig. 8), corroborates this concept. The CO_2 must have migrated as a separate phase and would have had the capacity to quantitatively partition any gases from the groundwater phase into the CO_2, effectively 'stripping' the groundwater of its dissolved gas content. This would produce a CO_2 reservoir with an ASW-like composition that would also have contained any radiogenic-crustal noble gases that the stripped groundwater had accumulated. At this stage the groundwater is saturated with respect to CO_2, but is completely depleted with respect to the atmosphere-derived noble gases (Fig. 9).

Subsequent charges of magmatic CO_2 would then pass through the gas stripped groundwater but serve only to dilute the ASW-derived and crustal-radiogenic noble gases in the CO_2 trapping structure. Bravo Dome preserves a clear ^{20}Ne concentration gradient, increasing from west to east in the field. We argue this both corroborates the model and requires the reservoir filling direction, which may still be ongoing (Baines and Worden, 2004), to be from the west.

The noble gases in the gas phase can then re-equilibrate with any degassed groundwater. This re-equilibration will occur under either open system or closed system conditions depending on the available volume of water for re-equilibration and factors such as whether there is significant water movement or not. For open system conditions, the re-dissolution process will follow a Rayleigh fractionation path. Under closed system conditions, the fractionation trend will be the exact reverse of that calculated for batch fractionation of a gas phase exsolving from water. Using the Bravo Dome reservoir conditions, we show in Figure 7 that the open system Rayleigh fractionation re-dissolution model accounts for all of the mantle corrected $^{20}Ne/^{36}Ar_{(atm)}$ and $^{84}Kr/^{36}Ar_{(atm)}$ ratios that are observed in the field, with the exception of one sample (BD11). This occurs with coherent fractionation of the radiogenic noble gases that we argue are stripped from the groundwater at the same time as the ASW noble gases.

Using the open system re-dissolution model outlined above, the fractionation of the measured gas phase $^{20}Ne/^{36}Ar$ ratios from the groundwater value defines the proportion of ^{36}Ar lost from the gas phase into solution. It is then straightforward to calculate the initial concentration of ^{36}Ar, $^{36}Ar_{init}$, within the gas phase prior to the fractionating (re-dissolution) process (Table

3)(e.g. Zhou et al., 2005). From the concentration of ^{36}Ar in ASW we then calculate for each sample the volume of water required to have been gas 'stripped' to supply the $^{36}Ar_{init}$ and present this as the Stage 1 Water/Gas volume ratio. For the Bravo Dome system, Stage 1 Water/Gas volume ratio ranges from 0.0005 to 0.071 cm^3 of water per cm^3 gas (STP) (Table 3). Under reservoir conditions 1 cm^3 of groundwater can hold 4.66 cm^3 of CO_2 (STP) in solution (Spycher and Preuss, 2005). This results in a Water/Gas ratio of 0.215 and is far higher than the largest estimated Stage 1 V_{Water}/V_{Gas} Bravo Dome value. This is consistent with the CO_2 gas charging the reservoir as a separate and distinct phase, and therefore with the gas 'stripping' conceptual model proposed (Fig. 9).

It is trivial to then calculate the volume of water, under reservoir conditions (Table 4), that the gas phase noble gases must re-dissolve into in order to fractionate the $^{20}Ne/^{36}Ar$ values from ASW (0.152) to that observed. For the Bravo Dome system this varies from zero to 104 cm^3 water per cm^3 gas (RTP) (RTP = Reservoir Temperature and Pressure) (Table 3), which corresponds to zero to 1.51 cm^3 water per cm^3 gas (STP). The volume of degassed water required to fractionate the $^{20}Ne/^{36}Ar$ from ASW to observed values is far larger than the volume of water 'stripped' to supply the gases, by up to a factor of 50. Little, if any, CO_2 will dissolve in this water while it remains CO_2 saturated. For the first time we quantify on a sample by sample basis the volume of water the gas in this CO_2 storage analogue has interacted with both i) on reservoir filling; and ii) subsequent to reservoir filling.

5.1.2. Sheep Mountain

We have already noted from the lack of correlation of radiogenic noble gases with the ASW-derived $^{20}Ne/^{36}Ar$ that the reservoir fluid history at Sheep Mountain is more complex than in the other fields studied. It is interesting to note that the groundwater salinity in this field is significantly lower than that of the other fields too (Table 4), possibly indicating an influence from younger less saline fluids. Nevertheless, In Figure 10a we show that the $^{20}Ne/^{36}Ar$ ratios in the Sheep Mountain gases can also be accounted for by the re-dissolution of a gas phase with an initial gas composition of ASW, consistent with the model described for Bravo Dome. The model predicted $^{84}Kr/^{36}Ar$ values are below those observed (Fig. 10a). This could be explained by a higher initial groundwater excess air component or a sedimentary excess-air ^{84}Kr, possibly sourced from hydrocarbons associated with the nearby Oakdale natural gas

field (Worrall, 2004). The lack of any spatial ^{20}Ne concentration trend within the field suggests that any filling history has not been preserved.

For comparison we use the extent of fractionation of $^{20}Ne/^{36}Ar$ from ASW values to determine the original $^{36}Ar_{init}$ abundances prior to the re-dissolution stage and calculate the volume of groundwater 'stripped' for each sample (Table 3). These values range from 0.025 cm^3 to 2.32 cm^3 water per cm^3 gas (STP)(Table 4), significantly higher than the Bravo Dome values. The volume of water required to fractionate the $^{20}Ne/^{36}Ar$ from ASW to observed values under reservoir conditions (Table 4) assuming an open system range from 48.6 to 114 cm^3 water per cm^3 gas (RTP), with the four most extreme fractionated gas requiring 144 to 175 cm^3 water per cm^3 gas (RTP)(Table 3). Excluding the four extreme samples, the reservoir condition Gas/Water volume ratio range for the reservoir re-equilibration is similar to that of Bravo Dome.

5.1.3. McCallum Dome

$^{20}Ne/^{36}Ar$ values within this field can also be explained by the re-dissolution of noble gases into a previously stripped groundwater (Fig. 10b). Similar to Sheep Mountain, the observed $^{84}Kr/^{36}Ar$ ratios are however, higher than the re-dissolution model predicts. This could be explained by an addition of approximately 70% excess Kr (Fig. 10b). Like Sheep Mountain, McCallum Dome is proximal to local hydrocarbon production and we speculate that the excess Kr may be related to sedimentary Kr released on the decomposition of the source kerogen (Torgersen and Kennedy, 1999). Using the fractionation of $^{20}Ne/^{36}Ar$ from ASW, the volume of stripped groundwater required to account for the $^{36}Ar_{init}$ abundance prior to re-dissolution ranges from 0.21 to 0.60 cm^3 water per cm^3 gas (STP), similar to the upper values at Sheep Mountain (Table 3). The volume of water required to fractionate the $^{20}Ne/^{36}Ar$ from ASW to observed values under reservoir conditions (Table 5) assuming an open system range from 49 to 86 cm^3 water per cm^3 gas (RTP), similar to the volumes calculated for Bravo Dome and Sheep Mountain.

5.1.4. St. John's Dome

The observed $^{20}Ne/^{36}Ar$ ratios in the St. John's Dome samples are close to the calculated ASW value of 0.152. This implies that limited re-equilibration of noble gases has occurred since the groundwater was stripped of its ASW composition. $^{84}Kr/^{36}Ar$ ratios from the St.

John's field are also close to the ASW value of 0.045. Using the re-dissolution model and average reservoir conditions (Table 4), the volume of groundwater stripped on reservoir filling varies from 0.15 to 2.5 cm^3 water per cm^3 gas (STP), while re-equilibration requires zero to 31 cm^3 water per cm^3 gas (RTP) (Table 3). In a similar fashion to Bravo Dome, St. Johns Dome preserves a marked ^{20}Ne concentration gradient, increasing from the centre of the trapping structure next to the Coyote Wash fault to the margin of the structure in the north (appendix). We argue that this is the result of the dilution of ASW noble gases by magmatic CO_2 injection within the centre of the reservoir implying that the reservoir was filled by CO_2 migrating into the reservoir via the Coyote Wash fault.

5.1.5 *McElmo Dome*

As mentioned previously McElmo Dome $^{20}Ne/^{36}Ar$ values are the only ones to significantly fall below the nominal ASW value of 0.152, by as much as 30%. $^{84}Kr/^{36}Ar$ values also exhibit a greater variation than observed in other fields ranging from 0.02 to a maximum ratio of 0.072. While the latter could be accounted for by an excess ^{84}Kr component, this would not account for the low $^{20}Ne/^{36}Ar$, suggesting some degree of perturbation of the groundwater system prior to stripping. With this caveat, we nevertheless calculate $^{36}Ar_{init}$ assuming an unperturbed ASW. The volume of ASW required to account for the $^{36}Ar_{init}$ varies from 0.011 cm^3 to 0.49 cm^3 water per cm^3 gas (STP) (Table 3). The re-dissolution groundwater volumes range from zero to 91 cm^3 water per cm^3 gas (RTP) and are within the range of all other fields.

6.0 SUMMARY

Geological CO_2 sequestration requires the safe storage of CO_2 on a timescale in the region of a 1 ka to 10 ka (Haszeldine et al., 2005). The long-term consequences of increasing the gross volume of CO_2 in the crust must be identified in order for geologic CO_2 sequestration to be proven as a safe and viable method to reduce emissions of this greenhouse gas. Identification of the source of CO_2 in natural reservoirs and development of physical models to account for the migration and interaction of this CO_2 with the groundwater is essential for developing a quantitative understanding of the long term storage potential of CO_2 in the subsurface. The Bravo Dome, Sheep Mountain, St Johns Dome and McCallum Dome CO_2 fields in the Colorado Plateau and Rocky Mountain provinces, USA provide a key set of analogues.

The $CO_2/^3He$ values of all of the well gas samples show that the CO_2 in each of the separate reservoirs has a significant, if not dominant magmatic component. The magmatic activity related to all of the fields dates from late Tertiary through to the late Quaternary (Appendix). The most recent magmatic events related to the natural gas fields studied occurred in the Raton-Clayton volcanic field close to Bravo Dome between 10 ka and 8 ka (Broadhead, 1998). The next youngest is associated with St. John's Dome; the last phase of volcanic activity from the nearby Springerville Volcanic field dates from 0.3 to 2.1 Ma (Rauzi, 1999). Magmatic activity associated with both the Sheep Mountain and McCallum Dome fields is older, dating from the Late Tertiary (Maughan, 1988; Woodward, 1983). The oldest intrusive igneous rocks in the study are those associated with McElmo Dome, from the nearby Ute Mountain and La Plata Mountain laccoliths which have been dated at 40 – 72 Ma (Stevens et al., 2004). These ages have been determined on surface intrusive igneous rocks. It is probable that deep igneous activity will have continued for a significant period after these surface rocks were formed. However, the dates provide a crude estimation of the CO_2 residence time in the reservoir and imply millions of year timescales for CO_2 residence in these fields.

We have shown that a common two stage groundwater gas stripping and re-dissolution model (Fig. 9), can explain the first order trends observed in the air derived noble gas isotopes in all CO_2 reservoirs studied. This model allows us to quantify on a sample by sample basis the volume of water originally 'gas stripped' during reservoir filling and the volume of groundwater the gas in the reservoir has subsequently interacted with. In detail, perturbation of the original groundwater or sedimentary contributions to Kr may explain where there is a mismatch in some fields between model and observation. The original field Gas/Groundwater ratio clearly controls the degree to which magmatic signatures are resolvable from accumulated crustal gases and dissolved air within the groundwater. This value is highly variable from one system to another. Where the original field Gas/Groundwater ratio varies systematically across a single field, this is most likely caused by dilution caused by subsequent charges of CO_2 that do not contain any ASW-derived noble gases and therefore preserves a record of reservoir filling direction. Different initial Gas/Groundwater ratios may play a fundamental role in determining the relative abundance of CO_2 to other species and its isotopic composition prior to reservoir filling, but is beyond the scope of this work. While the degree of gas/water

interaction subsequent to reservoir filling is variable across individual fields, the maximum volume of water that samples have interacted with is, under reservoir conditions, remarkably similar in all fields.

Acknowledgements

This research was supported by a NERC funded PhD studentship to SMVG. We extend thanks to all of the field operators for permission to sample the gas reservoirs and assistance with the background geology, particularly Larry Nugent of BP (Sheep Mountain), Theresa Muhic and Daniel Miller of Iron Creek Energy Group and Gary Grove of Bonanza Creek (McCallum Dome) and Tom White of Rigdeway Petroleum (St. John's Dome). Bev Clementson is thanked for extensive help in the laboratory and in assistance in obtaining field collection equipment. Reviews from Anne Battani, Johana Lippmann-Pipke and one anonymous reviewer greatly improved the manuscript.

References

Allis R., Chidsey T., Gwynn W., Morgan C., White S., Adams M. and Moore J. (2001) Natural CO_2 Reservoirs on the Colorado Plateau and Southern Rocky Mountains: Candidates for CO_2 sequestration. *DOE/NETL: 1st National Conference of Carbon Sequestration.* **Proceedings Volume**.

Baars D. L. (2000) *The Colorado Plateau: A Geologic History*. University of New Mexico Press.

Baines S. J. and Worden R. H. (2004) The long term fate of CO_2 in the subsurface: natural analogues for CO_2 storage. In *Geological Storage of Carbon Dioxide*, Vol. 233 (ed. S. J. Bains and R. H. Worden), pp. 59-85. Geological Society.

Ballentine C. J., Burgess R. and Marty B. (2002) Tracing fluid origin, transport and interaction in the crust. In *Noble Gases in Geochemistry and Cosmochemistry*, Vol. 47 (ed. D. R. Porcelli, C. J. Ballentine, and R. Weiler), pp. 539-614.

Ballentine C. J. and Burnard P. G. (2002) Production, release and transport of noble gases in the continental crust. In *Noble Gases in Geochemistry and Cosmochemistry*, Vol. 47 (ed. D. R. Porcelli, C. J. Ballentine, and R. Weiler), pp. 481-538.

Ballentine C. J., Marty B., Lollar B. S. and Cassidy M. (2005) Neon isotopes constrain convection and volatile origin in the Earth's mantle. *Nature* **433**, 33-38.

Ballentine C. J., O'Nions R. K. and Coleman M. L. (1996) A Magnus opus: Helium, neon, and argon isotopes in a North Sea oilfield. *Geochimica et Cosmochimica Acta* **60**(5), 831-849.

Ballentine C. J., O'Nions R. K., Oxburgh E. R., Horvath F. and Deak J. (1991) Rare-gas constraints on hydrocarbon accumulation, crustal degassing and groundwater-flow in the Pannonian Basin. *Earth and Planetary Science Letters* **105**(1-3), 229-246.

Ballentine C. J., Schoell M., Coleman D. and Cain B. A. (2001) 300-Myr-old magmatic CO_2 in natural gas reservoirs of the west Texas Permian basin. *Nature* **409**, 327-331.

Ballentine C. J. and Sherwood Lollar B. (2002) Regional groundwater focusing of nitrogen and noble gases into the Hugoton-Panhandle giant gas field, USA. *Geochimica et Cosmochimica Acta* **66**(14), 2483-2497.

Ballentine C. J., Mazurek M. and Gautschi A. (1994) Thermal constraints on crustal rare gas release and migration: Evidence from Alpine fluid inclusions. *Geochimica et Cosmochimica Acta* **58**, 4333-4348

Battani A., Sarda P. and Prinzhofer A. (2000) Basin scale natural gas source, migration and trapping traced by noble gases and major elements: the Pakistan Indus basin. *Earth and Planetary Science Letters* **181**(1-2), 229-249.

Biggs P. (1957) CO_2 at North and South McCallum. In *Guidebook to the geology of North and Middle Parks Basin, Colorado* (ed. W. C. Finch), pp. 92-93. Rocky Mountain Association of Geologists, 9th Annual Field Conference.

Bosch, A. and E. Mazor (1988) Natural gas association with water and oil depicted by atmospheric noble gases: case studies from the southern Mediterranean Coastal Plain. *Earth Planet. Sci. Lett.* **87**, 338 - 346.

Broadhead R. F. (1993) Carbon dioxide in northest New Mexico. *West Texas Geological Society Bulletin* **32**, 5-8.

Broadhead R. F. (1998) Natural accumulations of carbon dioxide in the New Mexico region - Where are they, how do they occur and what are the uses for CO_2? *Lite Geology* **20**, 2-6.

Caffee M. W., Hudson G. U., Velsko C., Huss G. R., Alexander E. C. and Chivas A. R. (1999) Primordial noble cases from Earth's mantle: Identification of a primitive volatile component. *Science* **285**, 2115-2118.

Cappa J. and Rice D. (1995) Carbon dioxide in Mississpian rocks of the Paradox Basin and adjacent areas, Colorado, Utah, New Mexico and Arizona. *U.S. Geological Survey Bulletin No. 2000-H*.

Carpen T. R. (1957a) North McCallum Field, Jackson County, Colorado. In *Guidebook to the geology of North and Middle Parks Basin, Colorado* (ed. W. C. Finch), pp. 109-112. Rocky Mountain Association of Geologists, 9th Annual Field Conference.

Carpen T. R. (1957b) South McCallum Field, Jackson County, Colorado. In *Guidebook to the geology of North and Middle Parks Basin, Colorado* (ed. W. C. Finch), pp. 113-114. Rocky Mountain Association of Geologists, 9th Annual Field Conference.

Cassidy, M. (2005) Occurrence and origin of free carbon dioxide gas deposits in the earth's continental crust. PhD Thesis, University of Houston, Texas.

Crovetto R., Fernandez-Prini R. and Laura Japas M. (1982) Solubilities of inert gases and methane in H_2O and in D_2O in the temperature range of 300 to 600K. *Journal of Chemical Physics* **76**, 1077-1086.

Fanale F. P. and Cannon W. A. (1971) Physical adsorption of rare gases on terrigenous sediments. *Earth and Planetary Science Letters* **11**, 362-368.

Fitton J. G., James D. and Leeman W. P. (1991) Basic Magmatism Associated with Late Cenozoic Extension in the Western United-States - Compositional Variations in Space and Time. *Journal of Geophysical Research-Solid Earth and Planets* **96**(B8), 13693-13711.

Gerling C. R. (1983) McElmo Dome Leadville Carbon Dioxide Field, Colorado. In *Oil an Gas fields of the Four Corners Area*, Vol. 3 (ed. J. E. Fassett), pp. 735-739. Four Corners Geological Society.

Haszeldine R. S., Quinn O., England G., Wilkonson M., Shipton Z. K., Evans J. P., Heath J. E., Crossey L., Ballentine C. J. and Graham C. M. (2005) Natural geochemical analogues for carbon dioxide torage in deep geological porous reservoirs, a UK perspective. In *Special Issue Oil and Gas Science and Technology (Revue de Inst Francais de Petrole)*, Vol. 60 (ed. E. Brosse), pp. 33-49.

Hennecke E. W. and Manuel O. K. (1975) Noble gases in CO_2 Well Gas, Harding County, New-Mexico. *Earth and Planetary Science Letters* **27**(2), 346-355.

Hilton, D.R., Fischer, T.P. and Marty, B. (2002) Noble gases and Volitile Recycling at Subduction Zones. In *Noble Gases in Geochemistry and Cosmochemistry*, Vol. 47 (ed. D. R. Porcelli, C. J. Ballentine, and R. Weiler), pp. 319-370.

Holland G. and Ballentine C. J. (2006) Seawater subduction controls the heavy noble gas composition of the mantle, *Nature* **441,** 186-191.

International Panel on Climate Change. (1996) Climate Change 1995: The Science of Climate Change, Summary for Policymakers and Technical Summary of the Working Group I report, pp. 56pp. Cambridge University Press, Cambridge, UK.

International Panel on Climate Change. (2001) Climate Change 2001: The Scientific Basis, Summary for Policymakers and Technical Summary of the Working Group I Report. Cambridge University Press, Cambridge, UK.

International Panel on Climate Change. (2007). Climate change 2007: Mitigation. Contribution of Working group III to the Fourth Assessment Report of the Intergovernmental Panel on Climate Change. B. Metz, O. R. Davidson, P. R. Bosch, R. Dave, L. A. Meyer (eds), Cambridge University Press, Cambridge, United Kingdom and New York, NY, USA.

Jenden P. D., Hilton D. R., Kaplan I. R. and Craig H. (1993) Abiogenic hydrocarbons in and mantle helium in oil and gas fields. In *The future of energy gases, U.S. Geological Survey Professional Paper 1570* (ed. D. G. Howell), pp. 31-56. U.S. Geological Survey.

Johnson R. E. (1983) Bravo Dome carbon dioxide area, North east New Mexico. In *Oil and Gas Fields of the Four Corners area*, Vol. 3 (ed. J. E. Fassett), pp. 745-748. Four Corners Geological Society.

Johnston R. B. (1959) Geology of Huerferno Park Area, Huerferno and Custer County, Colorado. *U.S. Geological Survey Bulletin No. 1071-D*.

Kennedy B. M., Hiyagon H., and Reynolds J. H. (1990) Crustal Neon - A Striking Uniformity. *Earth And Planetary Science Letters* **98**(3-4), 277-286.

Kennedy B. M., Torgersen T. and van Soest M. C. (2002) Multiple atmospheric noble gas components in hydrocarbon reservoirs: A study of the Northwest Shelf, Delaware Basin, SE New Mexico. *Geochimica et Cosmochimica Acta* **66**(16), 2807-2822.

King M. B., Mubarak A., Kim J. and Bott T. (1992) The Mutual Solubilities of Water with Supercritical and Liquid Carbon Dioxide. *The Journal of Supercritical Fluids* **5**, 296-302.

Kipfer R., Aeschbach-Gertig W., Peeters F. and Stute M. (2002) Noble gases in lakes and groundwaters. In *Noble Gases in Geochemistry and Cosmochemistry*, Vol. 47, pp. 615-700.

Kron, A. and Heiken, G. (1980) Geothermal Gradient Map of the United States. In: *Geothermal Resources Council, 1980 Annual Meeting, Transactions,* **Vol. 4**

Marty B. and Jambon A. (1987) C/^{3}He in volitile fluxes from the solid Earth: Implications for carbon geodynamics. *Earth and Planetary Science Letters* **83**, 16-26.

Matsubara K. and Matsuda J. (1995) Laboratory experiments on the Ne enrichments in terrestrial natural glasses. *Geochemistry Journal* **29**, 293-300.

Matsuda J.I., Matsubara K., Yajima H. and Yamamoto K. (1989) Anomalous Ne enrichment in obsidians and Darwin glass: Diffusion of noble gases in silica-rich glasses. **53**(11), 3025.

Maughan E. K. (1988) Geology and Petroleum Potential, Colorado Park Basin Province, North-Central Colorado. *U.S. Geological Survey Open-File Report 88-450 E*.

Parsons T. and McCarthy J. (1995) The active southwest margin of the Colorado Plateau: uplift of mantle origin. *Geological Society of America Bulletin* **107**(2), 139-147.

Phinney D., Tennyson J. and Frick U. (1978) Xenon In CO_2 Well Gas Revisited. *Journal of Geophysical Research* **83**(NB5), 2313-2319.

Pinti D. L. and Marty B. (1995) Noble-Gases In Crude Oils From The Paris Basin, France - Implications For The Origin Of Fluids And Constraints On Oil- Water-Gas Interactions. *Geochimica et Cosmochimica Acta* **59**(16), 3389-3404.

Pinti D. L., Wada N. and Matsuda J. (1999) Neon excesses in pumice: Volcanological implications. *Journal of Volcanology and Geothermal Research* **88**, 279-289.

Prinzhofer A., Vega M. A. G., Battani A. and Escudero M. (2000) Gas geochemistry of the Macuspana Basin (Mexico): thermogenic accumulations in sediments impregnated by bacterial gas. *Marine and Petroleum Geology* **17**(9), 1029-1040.

Rauzi S. L. (1999) Carbon dioxde in the St. John's - Springerville Area, Apache County, Arizonia. *Arizonia Geological Survey, Open-File Report 99-2*.

Roth G. (1983) Sheep Mountain and Dike Mountain Fields, Huerfano County, Colorado; A source of CO_2 for enhanced oil recovery. In *Oil and Gas Fields of the Four Corners Area*, Vol. 3 (ed. J. E. Fassett), pp. 740-744. Four Corners Geological Society.

Sherwood Lollar B., Ballentine C. J. and O'Nions R. K. (1997) The fate of mantle-derived carbon in a continental sedimentary basin: Integration of C/He relationships and stable isotope signatures. *Geochimica et Cosmochimica Acta* **61**(11), 2295-2308.

Sherwood Lollar B., Slater G. F., Ahad J., Sleep B., Spivack J., Brennan M. and MacKenzie P. (1999) Contrasting carbon isotope fractionation during biodegradation of trichloroethylene and toluene: Implications for intrinsic bioremediation. *Organic Geochemistry* **30**("Part 1"), 813-820.

Shipton Z. K., Evans J. P., Kirschner D., Kolesar P. T., Williams A. P. and J H. (2004) Analysis of leakage through 'low-peameability' faults from natural reservoirs in the Colorado Plateau, east-central Utah. In *Geological Storage of Carbon Dioxide*, Vol. 233 (ed. S. J. Baines and R. H. Worden), pp. 43-58. Geological Society.

Spycher, N. and Pruess, K. $CO_2 – H_2O$ mixtures in the geological sequestration of CO_2. II Partitioning in chloride brines at 12 – 100°C and up to 600 bar. *Geochimica et Cosmochimica Acta,* **69** No. 13, 3309-3320.

Stevens S. H., Fox C., White T. and Melzer S. (2004) Natural CO_2 analogs for Carbon Sequestration. *Midterm Report for USDOE*.

Stevens S. H., Pearce J. M. and J R. A. A. (2001) Natural Analogues for Geologic Storage of CO_2: An Integrated Global Research Program. *First National Conference on Carbon Sequestration*.

Torgersen T., Kennedy B. and van Soest M. (2004) Diffusive separation of noble gases and noble gas abundance patterns in sedimentary rocks. *Earth and Planetary Science Letters* **226**(3-4), 477-489.

Torgersen T. and Kennedy B. M. (1999) Air-Xe enrichments in Elk Hills oil field gases: role of water in migration and storage. *Earth and Planetary Science Letters* **167**(3-4), 239-253.

Woodward L. A. (1983) Geology and Hydrocarbon Potential of the Raton Basin, New Mexico. In *Oil and Gas Fields of the Four Corners Area*, Vol. 3 (ed. J. E. Fassett), pp. 789-799. Four Corners Geological Society.

Worrall, J. (2004) Preliminary Geology of Oakdale Field, Northwest Raton Basin, Huerfuno County, Colorado. Search and Discovery Article #20017.

Wycherley H., Fleet A. and Shaw H. (1999) Some observations on the origins of large volumes of carbon dioxide accumulations in sedimentary basins. *Marine and Petroleum Geology* **16**(6), 489-494.

Zartman R. E., Reynolds J. H. and Wasserburg G. J. (1961) Helium argon, and carbon in some natural gases. *Journal of Geophysical Research* **66**(1), 277-306.

Zhou Z., Ballentine C. J., Kipfer R., Schoell M. and Thibodeaux S. (2005) Noble gas tracing of groundwater/coalbed methane interaction in the San Juan Basin, USA. *Geochimica et Cosmochimica Acta* **69**(23), 5413-5428.

Appendix

A1. Bravo Dome

The Bravo Dome field (originally named the Bueyeros field) is located south of Cortez in Harding County, northeast New Mexico (Fig. 1; A1). The field is a large (2000 km^2) northwest trending anticlinal nose situated on the spur of the Sierra Grande arch (Baines and Worden, 2004). The region is bounded by the Tucumari basin to the south and the Dalhart Basin to the north (Baars, 2000; Johnson, 1983).

Bravo Dome produces almost pure (99%) CO_2 from the Tubb formation at depths of 600 to 700 m with an average thickness of 30 m (Broadhead, 1993; Broadhead, 1998; Stevens et al., 2001). This is an arkosic sandstone of Permian age and was formed by sand-dominated alluvial, fluvial and aeolian deposition. CO_2 is trapped by a combination of stratigraphic pinch-out, fold closure and possibly hydrodynamic forces. The reservoir is sealed by the impervious Cimarron Anhydrite which is a mix of shallow marine evaporates and arkosic muds (Baines and Worden, 2004; Broadhead, 1993; Broadhead, 1998). Average porosity and permeability are 20% and 42 mD respectively (Allis et al., 2001). Total reserves are estimated to be 450 billion m^3 (Allis et al., 2001). The CO_2 is believed to have migrated from vents associated with the nearby Rio Grande rift volcanic activity. Known volcanic activity in the region dates from 10,000 to 8,000 years ago suggesting that the field filled recently (Broadhead, 1998 and Cassidy, 2005). CO_2 migration into the field may still be ongoing, as indicated by a significant pressure increase (29 kPa) in an isolated shut in well over the last decade (Baines and Worden, 2004).

A2. Sheep Mountain

The Sheep Mountain gas field is located at the northern end of the Raton Basin, 45 km northwest of the town of Walsenberg, south central Colorado (Fig. 1; A2). The surrounding region, Huerfano Park, is bounded on the west by the Sangre de Cristo Mountains and on the east by the Wet Mountains. The Raton Basin stretches some 175 miles to the south, from southern Colorado and northern New Mexico. The sedimentary sequence in the region ranges from Pennsylvanian through to Tertiary in age, and lies under and east of the Paldura thrust sheet (Woodward, 1983). Folding and overthrusting induced by this thrust created the Malachite syncline and the little Sheep Mountain anticline. This northwest trending anticlinal fold is bounded on the northeast side by a minor thrust fault and forms the structural trap of the field (Fig. A3). The reservoir produces almost pure CO_2 (~97%) from the Cretaceous Dakota and Jurassic Entrada sandstones at depths of 1400 m to 1800 m. Porosity within the reservoir varies from 16 - 20%, roughly twice the typical porosity of the Dakota and Entrada of 6-

10% (Worrall, 2004). This is believed to be because the sandstones within the folded thrust sheet are not subjected to silicification reactions related to groundwater recharge. This is because the Dakota and Entrada sandstones contained within the Sheep Mountain thrust sheet do not outcrop on the west side of the Raton basin, where groundwater recharge primarily occurs (Worrall, 2004). The field is relatively small (20 km^2) and contains 70 billion m^3 of CO_2 (Stevens et al., 2001).

The local igneous rocks are related to normal faulting of the province which accompanied upwarping in late Tertiary time. During this period large volumes of volcanic rock were extruded from vents along the Sierra Grande arch, within the Raton Basin and on the eastern margin of the basin. Major intrusives accompanied this volcanic activity, producing extensive sills and laccoliths (Woodward, 1983). The distinctive peaks of Little Sheep Mountain, Sheep Mountain and Dike Mountain are the result of laccoliths intruded during this period. The Sheep Mountain – Little Sheep Mountain laccolith trends north-northwest covering an area of approximately 13 km^2. The rocks are light grey, phaneritic to aphinitic, intermediate-acidic igneous rocks and are named as a monzonite porphyry (Johnston, 1959; Roth, 1983; Woodward, 1983). Prior to this work the CO_2 source was thought to be due to the thermal breakdown of carbonates as a result of the nearby intrusives (Caffee et al., 1999).

A3. McCallum Dome

McCallum dome is a comparatively small field situated in the North Park basin, northern Colorado (Fig 1). The field is comprised of two large anticlines, North McCallum Dome which is some 6 km northeast of the town of Walden and the faulted en-echelon South McCallum Dome that lies some 2 km to the southeast of the North Dome (Carpen, 1957a; Carpen, 1957b). The CO_2 is trapped in late Laramide related anticlines and faulted anticlines, as a result of a combination of structural and stratigraphic traps (onlap pinch-outs) (Maughan, 1988). The field produces CO_2 from the Lower Cretaceous Dakota and Lakota sandstones and has produced from the stratigraphically lower Morrison sands in the past (Carpen, 1957a). The reservoirs are relatively deep ranging from 1500 to 1900 m. Hydrocarbons are also produced from the field, sourced from the Perrie B shale reservoir which is typically 1 km above the Dakota/Lakota CO_2 reservoir. Small quantities of oil have been documented in the Lakota reservoir above the Gas/Water contact. The most prolific producer is the Dakota Sandstone which has an average thickness of 7-12 m, an average porosity of 15.7% and permeability of 70 mD (300 mD max). The Lakota sandstone is a coarser grained rock, and hence has a higher average porosity of 18.5% and an average permeability of 100 mD (450 mD max.) (Maughan, 1988). The field was first discovered in 1925 and has steadily produced small quantities of CO_2 since 1927. Cumulative production to 1999 is believed to be 19.5 billion m^3 (Allis et al., 2001). Currently four wells are in operation with the field producing around 1.076 billion m^3 per year of CO_2 for industrial use

Tertiary volcanic and terrigenous clastics lie unconformably on top of the Cretaceous sediments in the vicinity of the field. These were produced at the start of the Oligocene as a result of the main episode of the Laramide Orogeny. Evidence for high heat flow in the area dates from the Late Tertiary and is expressed by local hydrothermal mineralization. The province is believed to still have an elevated geothermal gradient as indicated by the presence of active thermal springs (Maughan, 1988). Prior to this work, thermal breakdown of carbonates as a result of this high heat flow regime had been highlighted as the most probable source of the CO_2 (Biggs, 1957; Maughan, 1988).

A4. McElmo Dome

McElmo Dome is a large (800 km^2) anticline situated at the south eastern end of the Paradox Basin in the Four Corners area of southwest Colorado (Fig. 1). The field is 35 km southeast of Cortez and just north of Ute Mountain. A small related field, Doe Canyon, lies some 5 km to the northwest. As the field is located in the centre of the Colorado Plateau, the surrounding surface geology is dominated by flat-lying sedimentary stratigraphy. The field is the world's largest known supply of commercial CO_2 (Stevens et al., 2001). CO_2 is contained in a supercritical state within the Carboniferous (Mississippian) Leadville limestone which is some 100 m thick. The reservoir structure is complex, consisting of interbedded porous permeable dolomite and tight limestones and ranges in depth from 1,800 to 2,600 m (Fig. A3). CO_2 is trapped by a combination of structural closure, permeability barriers within the Leadville Formation, CO_2-groundwater contact and a 400 m thick salt cap rock of the Paradox Formation. Porosity within the field varies from 3.5% to 25%, averaging 11% and permeability averages 23 mD (Stevens et al., 2001). The field was discovered in 1948 and is estimated to contain 476 billion m^3 of CO_2 (Allis et al., 2001). The CO_2-groundwater contact tilts west at an approximate gradient of 10 m/km, which is believed to be the result of local hydrodynamic conditions within the Leadville Formation resulting in the field being filled to spill point (Gerling, 1983).

The igneous history of the surrounding area is dominated by intrusive rocks, including the Ute Mountain and La Plata Mountain laccoliths which lie a few km south and east of the field respectively. Both intrusions date from 40 - 72 Ma. Prior to this work, carbon isotope measurements have been used to suggest that the CO_2 in the McElmo Dome field is derived from the thermal breakdown of the Leadville limestone associated with heating caused by the nearby Ute Mountain intrusion (Cappa and Rice, 1995).

A5. St. John's Dome

St. John's Dome is a large (1,800 km^2), asymmetrical faulted anticline situated on the southern tip of the Colorado Plateau on the Arizona/New Mexico border. The field lies on the edge of the Holbrook

Basin, in the transition zone between the Colorado Plateau, Basin and Range and Rio Grande Rift tectonic provinces (Fig. 1, A4). This is part of the Mogollen slope which is comprised of Precambrian crystalline basement, Paleozoic through to Cenozoic age sediments and Cenozoic volcanics (Rauzi, 1999). CO_2 in the field is trapped in the Permian Supai Formation which is a predominantly fine-grained alluvial sandstone intercalated with siltstone, anhydrite and dolomite. The reservoir is dissected by a major reverse fault, named the Coyote Wash fault, and smaller plays which may have influenced the sourcing and trapping of the CO_2 (Rauzi, 1999). Cap rocks in the field are impermeable anhydrites which vertically separate the CO_2 into multiple zones. The reservoir is relatively shallow at 200 - 700 m and produces CO_2 from a gas state. Average reservoir porosity is 10% and permeability varies widely averaging 10 mD (Stevens et al., 2001). Estimated reserves are believed to be in the region of 445 billion m^3 (Stevens et al., 2001).

The Springerville Volcanic Field (SVF) lies approximately 50 km southwest of the St. John's field. The SVF field covers nearly 3,000 km^2, with a volume of 300 km^2 of lava from some 400 volcanic centres. This is one of many late Pliocene to Holocene, predominantly basaltic, volcanic fields which surrounds the southern margin of the Colorado Plateau (Baars, 2000). The field is characterized by two main types of mafic lavas: an older (5 - 6 Ma) Olivine pyretic basalt with an enriched lithospheric source and a younger (0.3 - 2.1 Ma) alkali basalt which reflects mixing between an enriched mantle source and an ocean-island type source (Rauzi, 1999). No igneous or volcanics were cored during exploration of the field and, prior to this work, the source of St. John's Field CO_2 had not been investigated in detail (Rauzi, 1999).

Fig. 1. Map of the Colorado Plateau illustrating the sites of major Cenozoic igneous provinces, location of the natural CO_2 reservoirs sampled and other CO_2 reservoirs within the region. (Modified from Allis et al., 2001).

Fig. 2. Plot of N_2 against ^4He concentration for the McElmo Dome, Doe Canyon and St. John's Dome fields, showing a positive correlation between N_2 and ^4He. This relationship is attributed to the gas phase (CO_2) stripping old groundwater containing accumulated ^4He and N_2 (Ballentine and Sherwood Lollar 2002).

Fig. 3. Plot of $CO_2/^3He$ against CO_2 concentration for all of the reservoirs studied. All error bars are smaller than printed symbols. The shaded region highlights the range of $CO_2/^3He$ values measured in pure magmatic samples (MORB). All of the samples from the deep gas fields plot within or below this range, indicating the presence of a significant quantity of magmatic ^3He, implying a mantle origin for the CO_2 within these fields (Sherwood Lollar et al.,1999; Ballentine et al., 2001).

Fig. 4. Plot of $^3He/^4He$ (R/R_a) against $^{40}Ar/^{36}Ar$ for all samples. The clear correlation between $^3He/^4He$ and $^{40}Ar/^{36}Ar$ within Bravo Dome contrasts with the lack of variation measured in both Sheep Mountain and McElmo Dome and the anti correlation observed in McCallum.

Fig. 5. Plot of $^{20}Ne/^{22}Ne$ ratio against $^{21}Ne/^{22}Ne$ for all samples. Bravo Dome exhibits mixing between a pre-mixed crust/air component and the mantle. St. Johns, Sheep Mountain and McCallum highlight mixing between a pre-mixed crust/mantle component and air. The distinct values measured from McElmo Dome show that this field contains the highest proportional contribution from crustal/radiogenic sources.

Fig. 6a. Plot of $^{20}Ne/^{36}Ar$ against $^{84}Kr/^{36}Ar$ for all reservoirs studied. The majority of the $^{20}Ne/^{36}Ar$ values lie close to the calculated ASW ratios. Sheep Mountain field shows extreme fractionation in $^{20}Ne/^{36}Ar$.

Fig. 6b. Plot of $^{84}Kr/^{36}Ar$ against $^{130}Xe/^{36}Ar$ for Sheep Mountain, McElmo Dome and Bravo Dome. The Xe and Kr systems are similar in both the McElmo Dome and Sheep Mountain fields. The extreme fractionation of $^{20}Ne/^{36}Ar$ observed in the Sheep Mountain field is not reflected in the other elemental ratios. Bravo Dome values are corrected for mantle contributions using $^{84}Kr/^{36}Ar_{mntl} = 0.051$ and $^{130}Xe/^{36}Ar_{mntl} = 0.001045$ (Ballentine et al., 2005).

Fig. 7. Plot of mantle corrected $^{20}Ne/^{36}Ar_{(atm)}$ against $^{84}Kr/^{36}Ar_{(atm)}$ for the Bravo Dome field. Also plotted are the Air and ASW values and the calculated Rayleigh and Batch fractionation curves for a gas phase exsolving from a groundwater that has an initial ASW composition (dashed lines). The tick marks on the dashed lines represent the proportion of Ar remaining in the groundwater phase. Also plotted is the Rayleigh fractionation line which would be produced by a gas phase dissolving into a water phase initially containing no noble gases (solid line). This is the re-dissolution model discussed in the text. The **bold** tick marks on the solid fractionation line represent the proportion of Ar lost from the gas phase. With the exception of the $^{84}Kr/^{36}Ar$ ratio of BD11, the fractionation pattern observed in the air derived ratios can be explained by the re-dissolution model.

Fig. 8. Plot of $^{20}Ne/^{36}Ar_{(atm)}$ against $^{20}Ne_{(atm)}$ for the samples from the Bravo Dome field. Also plotted are the predicted ^{20}Ne concentration values assuming Rayleigh Fractionation of a gas phase exsolving from the groundwater. The predicted concentrations are several orders of magnitude greater than the observed concentrations, implying that the atmospheric noble gases within the reservoir have been significantly diluted, most probably by injection of magmatic CO_2.

Fig. 9. Cartoon illustrating the two stage degassed groundwater and re-dissolution model. **Stage 1:** Magmatic CO_2 injection into the groundwater system causes the groundwater to become fully saturated in CO_2 with excess gas forming a free CO_2 gas phase. The free gas phase migrates upwards; stripping dissolved air-derived noble gases and accumulated crustal/radiogenic noble gases through CO_2/water phase partitioning. This produces a groundwater phase that is fully saturated in CO_2 and completely degassed with respect to ASW and crustal noble gases (and N_2). The CO_2 gas containing the groundwater stripped gases, on encountering a trapping structure, provides the first reservoir fluid charge. Subsequent charges of CO_2 provide no more ASW and crustal noble gases, and serve to dilute the original ASW and crustal noble gas rich CO_2. Reservoir scale preservation of concentration gradients in ASW-derived noble gases thus provide CO_2 filling direction (cf Bravo Dome, St Johns). **Stage 2:** When recharge of the gas cap stops, the noble gases will begin to re-dissolve into the gas stripped groundwater. This will result in a fractionation of the ASW-derived noble gases (Fig. 9). The magnitude of this fractionation will depend on the volume of water in contact with the gas phase and whether it is an open or closed system. Only limited CO_2 re-dissolution will occur caused for example, by a change in reservoir conditions or carbonate precipitation resulting in a reduction of the groundwater CO_2 saturation level.

Fig. 10a. Plot of $^{20}Ne/^{36}Ar$ against $^{84}Kr/^{36}Ar$ for the Sheep Mountain field. Also plotted are the calculated Rayleigh fractionation curve for a gas phase evolving from an ASW groundwater (dashed line) and the Rayleigh fractionation curve for gas with an ASW composition re-dissolving into degassed water containing no noble gases

(solid line). This second model accounts for the observed $^{20}Ne/^{36}Ar$. However the observed $^{84}Kr/^{36}Ar$ values are up to 4 times higher than predicted, possibly as a result excess sedimentary Kr and un-resolvable mantle contributions to ^{84}Kr. In both figures ASW and air values are also plotted.

Fig. 10b. Plot of $^{20}Ne/^{36}Ar$ against $^{84}Kr/^{36}Ar$ for the McCallum field. $^{20}Ne/^{36}Ar$ ratios can be explained by a similar model of re-dissolution of noble gases into a previously stripped groundwater as outlined for Bravo Dome and Sheep Mountain. $^{84}Kr/^{36}Ar$ ratios are significantly above those predicted by the model which we attribute to approximately 70% excess Kr associated with the source kerogen within the field. On both figures tick marks on the dashed line represent the proportion of Ar in the gas phase, whilst those on the solid re-dissolution line indicates the proportion of Ar lost to the groundwater.

Table 1. Sample location, producing formation and noble gas isotope ratios

Field & Well	Location Sec-Twp-Rge Or Lat-Long	Depth (m)	Producing Formation	$^{3}He/^{4}He$	$^{20}Ne/^{22}Ne$	$^{21}Ne/^{22}Ne$	$^{40}Ar/^{36}Ar$	$^{38}Ar/^{36}Ar$	$^{130}Xe/^{136}Xe$
McCallum	(North McCallum)								
No. 3 (8-3)	8/9N/78W	1618	Lakota	0.354 (7)	10.10 (9)	0.0627 (8)	7049 (51)	0.186 (2)	nm
No. 5	3/9N/79W	1520	Lakota	0.409 (7)	10.17 (8)	0.0615 (5)	3893 (34)	0.193 (11)	nm
No. 36	8/9N/79W		Dakota/Lakota	0.448 (8)	9.98 (6)	0.0500 (3)	2412 (17)	0.204 (4)	nm
No. 13	2/9N/79W	1625	Lakota/Morrison	0.393 (7)	10.02 (11)	0.0464 (4)	3434 (28)	0.195 (3)	nm
No. 79	4/9N/79W	1766	Dakota/Lakota	0.406 (6)	10.06 (6)	0.0454 (8)	3819 (41)	0.196 (3)	nm
Sheep Mtn									
8-2-P	2/9-28S/70W	1558	Dakota	0.981 (10)	10.14 (6)	0.0411 (4)	13839 (42)	0.184 (3)	0.422 (2)
2-10-O	15/9-27S/70W	1003	Entrada	0.984 (12)	10.08 (5)	0.0377 (2)	10745 (45)	0.185 (2)	0.421 (2)
9-26	26/9-27S/70W	1736	Dakota	0.934 (14)	10.19 (8)	0.0460 (3)	16486 (73)	0.185 (4)	0.417 (1)
2-9-H	9/9-27S/70W	930	Dakota	0.945 (19)	10.11 (6)	0.0311 (3)	4378 (23)	0.183 (6)	0.444 (4)
3-15-B	15/9-27S/70W	949	Dakota	0.937 (16)	10.11 (6)	0.0376 (3)	8746 (24)	0.187 (2)	0.430 (3)
4-13		1590	Dakota	0.942 (18)	10.20 (6)	0.0405 (3)	17314 (98)	0.186 (4)	0.416 (2)
4-26-E	26/9-27S/70W	1544	Entrada	1.024 (18)	10.29 (11)	0.0614 (3)	20783 (70)	0.185 (4)	0.412 (2)
3-23-D	22/9-27S/70W	1547	Dakota	0.988 (14)	10.15 (4)	0.0535 (3)	16812 (36)	0.185 (2)	0.418 (3)
7-35-L	2/9-28S/70W	1585	Dakota	0.916 (14)	10.23 (3)	0.0511 (3)	17594 (35)	0.186 (2)	0.414 (2)
2-35-C	26/9-27S/70W	1571	Dakota	0.963 (19)	10.29 (8)	0.0528 (3)	16574 (52)	0.183 (3)	0.426 (2)
1-15-C	15/9-27S/70W	1131	Entrada	0.967 (16)	9.94 (6)	0.0311 (3)	5194 (31)	0.185 (5)	nm
3-4-O	9/9-27S/70W	1201	Dakota	0.937 (14)	9.93 (9)	0.0342 (3)	4539 (11)	0.188 (2)	0.416 (3)
4-14-M	22/9-27S/70W	2015	Dakota	0.892 (15)	9.97 (6)	0.0404 (3)	17895 (175)	0.186 (8)	0.440 (1)
5-15-O	22/9-27S/70W	1427	Dakota	1.056 (15)	9.89 (6)	0.0319 (3)	8720 (26)	0.184 (3)	0.422 (2)
4-4-P	9/9-27S/70W	1058	Dakota	0.970 (14)	10.15 (8)	0.0440 (3)	16017 (40)	0.186 (3)	0.417 (2)
5-9-A	9/9-27S/70W	1023	Dakota	1.006 (18)	10.15 (3)	0.0428 (3)	17814 (41)	0.188 (3)	0.419 (1)
1-1-J	2/9-28S/70W	1656	Dakota	0.908 (16)	9.84 (3)	0.0407 (3)	12036 (24)	nm	nm
1-22-H	22/9-28S/70W	1528	Entrada	0.981 (17)	10.03 (2)	0.0401 (3)	10863 (70)	nm	nm
Bravo Dome									
BD01	23/19N/34E	653	Tubb	1.670 (8)	10.66 (3)	0.0562 (3)	10700 (314)	nm	nm
BD02	32/21N/35E	643	Tubb	0.764 (4)	9.96 (3)	0.0501 (3)	4654 (41)	nm	0.432 (1)
BD03	36/22N/34E	620	Tubb	0.896 (4)	10.01 (1)	0.0515 (1)	5342 (71)	nm	nm
BD04	8/20N/34E	670	Tubb	1.611 (8)	10.59 (4)	0.0541 (4)	9886 (185)	nm	0.419 (1)
BD05	34/20N/35E	644	Tubb	0.965 (5)	9.93 (1)	0.0526 (2)	5408 (38)	nm	0.430 (1)
BD06	26/22N/32E	648	Tubb	1.503 (8)	10.49 (4)	0.0561 (4)	9197 (161)	nm	nm
BD07	3/19N/33E	718	Tubb	2.104 (11)	11.20 (5)	0.0542 (4)	10923 (308)	nm	0.423 (2)
BD08	9/18N/33E	732	Tubb	1.143 (6)	10.21 (3)	0.0578 (4)	6643 (65)	nm	nm
BD09	17/21N/33E	659	Tubb	1.724 (9)	10.74 (5)	0.0578 (5)	nm	nm	nm
BD10	7/22N/34E	649	Tubb	1.104 (6)	10.20 (2)	0.0537 (3)	6719 (81)	nm	nm
BD11	25/19N/30E	640	Tubb	3.784 (19)	11.88 (5)	0.0565 (4)	21453 (1274)	nm	nm
BD12	27/19N/30E	604	Tubb	3.627 (18)			20888 (1017)	nm	nm
BD13	22/18N/35E	725	Tubb	1.318 (7)	10.25 (5)	0.0579 (5)	7714 (220)	nm	0.425 (1)
BD14	16/18N/34E	766	Tubb	1.413 (7)	10.54 (12)	0.0583 (2)	8490 (523)	nm	nm
BD12b	27/19N/30E	604	Tubb	3.634 (18)	11.60 (6)	0.0537 (2)	22492 (2474)	nm	nm
McElmo Dome									
Doe Canyon	37.7392, -108.8259	2439	Leadville	0.065 (1)	8.82 (8)	0.0788 (3)	8069 (15)	0.185 (1)	0.425 (2)
MC-1	37.4155, -108.7713	2543	Leadville	0.145 (2)	9.13 (12)	0.1044 (15)	15441 (30)	0.183 (1)	0.421 (2)
HE-2	37.5052, -108.9094	2443	Leadville	0.148 (1)	9.05 (5)	0.1119 (7)	14025 (141)	0.184 (3)	0.423 (2)
YC-4	37.4529, -108.8583	2349	Leadville	0.137 (3)	8.70 (7)	0.0910 (11)	2599 (5)	0.188 (1)	nm
SC-9	37.3934, -108.8733	2398	Leadville	0.150 (3)	8.62 (7)	0.1109 (13)	16296 (37)	0.186 (1)	0.418 (3)
YB-2	37.4472, -108.8075	2386	Leadville	0.125 (1)	8.90 (8)	0.1112 (6)	15513 (33)	0.188 (1)	0.423 (2)
YC-1	37.4529, -108.8583	2509	Leadville	0.142 (2)	8.94 (5)	0.1132 (5)	15148 (27)	0.182 (1)	nm
HF-1	37.4871, -108.8807	2533	Leadville	0.169 (1)	9.47 (10	0.0810 (9)	14058 (75)	nm	nm
HD-2	37.4572, -108.9008	2394	Leadville	0.140 (3)	8.42 (8)	0.1070 (11)	20231 (651)	nm	nm
YA-2	37.4692, -108.7811	2429	Leadville	0.138 (3)	8.48 (15)	0.1084 (20)	18497 (69)	nm	nm
YE-1	37.4818, -108.8123	2524	Leadville	0.173 (3)	8.84 (9)	0.1147 (13)	18515 (151)	nm	nm
HA-1	37.5289, -108.8718		Leadville	0.139 (3)	8.72 (5)	0.1062 (7)	18522 (85)	nm	nm
SC-10	37.3934, -108.8733	2455	Leadville	0.139 (2)	9.15 (8)	0.1071 (41)	21179 (54)	nm	nm
HC-2	37.4734, -108.8860	2451	Leadville	0.140 (2)	9.21 (7)	0.1069 (34)	24744 (96)	nm	nm
HB-1	37.5087, -108.8802	2435	Leadville	0.148 (3)	8.85 (5)	0.1061 (17)	22198 (144)	nm	nm
YD-1	37.4619, -108.8224	2439	Leadville	0.145 (3)	8.84 (5)	0.1006 (6)	19708 (91)	nm	nm
St. John's Dome									
22-1X	34.4265, -109.2664	655	Supai	0.455 (8)	9.75 (9)	0.0408 (2)	1369 (13)	0.197 (3)	nm
10-22	34.2437, -109.1645	690	Supai	0.394 (8)	9.71 (11)	0.0446 (2)	1492 (15)	0.197 (2)	nm
3-1	34.3771, -109.2563	553	Supai	0.433 (9)	9.80 (3)	0.0420 (3)	1687 (16)	0.193 (4)	nm

1σ errors to last significant figure in brackets, nm=not measured

Table 2. Gas Composition (%) and noble gas isotope concentrations (cm^3STP/cm^3)

Field & Well	CO_2 %	N_2 %	CH_4 %	C_2H_6 %	^4He (x 10^{-4}) $cm^3(STP)cm^{-3}$	^{20}Ne (x 10^{-8}) $cm^3(STP)cm^{-3}$	^{40}Ar (x 10^{-4}) $cm^3(STP)cm^{-3}$	^{84}Kr (x 10^{-10} $cm^3(STP)cm^{-3}$)	^{130}Xe (x 10^{-12}) $cm^3(STP)cm^{-3}$
McCallum	Mean gas	composition	from	producers					
No. 3 (8-3)	(92.1)	(0.34)	(5.0)	(0.39)	12.3 (2)	1.17 (2)	2.06 (1)	10.2 (3)	nm
No. 5	-	-	-	-	15.5 (2)	2.71 (3)	3.98 (2)	37.8 (7)	nm
No. 36	-	-	-	-	1.32 (12)	8.10 (8)	0.179 (8)	8.42 (5)	nm
No. 13	-	-	-	-	18.8 (2)	4.36 (5)	4.78 (2)	51.0 (5)	nm
No. 79	-	-	-	-	9.16 (21)	2.53 (3)	3.49 (2)	41.6 (4)	nm
Sheep Mtn	Mean gas	Composition	from	Allis et al., 2001					
8-2-P	(97.0)	(0.6)	(1.7)	-	3.13 (3)	1.47 (2)	1.69 (1)	3.03 (2)	4.76 (8)
2-10-O	-	-	-	-	2.96 (3)	3.04 (3)	1.62 (1)	3.10 (3)	4.65 (8)
9-26	-	-	-	-	2.95 (3)	0.613 (9)	1.57 (2)	2.60 (1)	4.11 (7)
2-9-H	-	-	-	-	3.07 (3)	9.77 (10)	1.39 (1)	5.54 (1)	8.93 (15)
3-15-B	-	-	-	-	2.90 (3)	1.54 (2)	1.60 (2)	3.98 (7)	6.50 (11)
4-13	-	-	-	-	3.47 (4)	1.11 (2)	2.08 (2)	2.75 (3)	5.63 (10)
4-26-E	-	-	-	-	3.15 (3)	0.442 (4)	1.73 (1)	1.66 (5)	4.47 (8)
3-23-D	-	-	-	-	3.17 (3)	0.579 (9)	1.84 (2)	1.62 (3)	3.27 (6)
7-35-L	-	-	-	-	3.06 (3)	0.749 (12)	1.56 (1)	4.49 (4)	5.22 (9)
2-35-C	-	-	-	-	2.87 (3)	0.573 (8)	1.57 (1)	2.71 (5)	4.79 (8)
1-15-C	-	-	-	-	2.71 (3)	6.77 (10)	1.55 (2)	6.49 (9)	nm
3-4-O	-	-	-	-	2.99 (3)	2.64 (3)	1.57 (1)	8.61 (5)	4.89 (9)
4-14-M	-	-	-	-	3.00 (3)	1.11 (1)	1.63 (2)	1.76 (6)	1.06 (17)
5-15-O	-	-	-	-	2.92 (3)	4.33 (5)	1.51 (1)	3.69 (3)	5.44 (9)
4-4-P	-	-	-	-	2.52 (2)	1.31 (2)	1.60 (2)	2.73 (5)	5.52 (10)
5-9-A	-	-	-	-	2.94 (3)	1.28 (2)	2.06 (1)	3.05 (5)	3.15 (6)
1-1-J	-	-	-	-	2.16 (2)	0.878 (12)	1.66 (1)	5.29 (9)	nm
1-22-H	-	-	-	-	3.22 (3)	0.937 (13)	1.55 (1)	5.72 (1)	nm
Bravo Dome	Mean gas	composition	from	Cassidy, 2006					
BD01	(99.6)	(0.20)	(0)	-	0.944 (12)	0.169 (2)	0.303 (3)	1.01 (2)	nm
BD02	-	-	-	-	4.15 (5)	0.700 (7)	0.652 (6)	5.04 (14)	9.83 (40)
BD03	-	-	-	-	3.31 (4)	0.521 (5)	0.536 (5)	3.24 (8)	nm
BD04	-	-	-	-	9.61 (2)	0.181 (2)	0.286 (3)	1.03 (3)	2.09 (9)
BD05	-	-	-	-	2.70 (4)	0.446 (4)	0.538 (5)	3.33 (8)	6.15 (25)
BD06	-	-	-	-	1.20 (2)	0.202 (2)	0.350 (3)	1.35 (4)	nm
BD07	-	-	-	-	0.781 (10)	0.180 (2)	0.280 (3)	0.900 (36)	1.96 (10)
BD08	-	-	-	-	1.61 (2)	0.264 (3)	0.396 (4)	2.00 (5)	nm
BD09	-	-	-	-	0.981 (12)	0.180 (2)	nm	nm	nm
BD10	-	-	-	-	1.99 (3)	0.308 (3)	0.396 (3)	2.02 (5)	nm
BD11	-	-	-	-	0.391 (5)	0.103 (1)	0.241 (4)	0.455 (19)	9.94 (9)
BD12	-	-	-	-	0.415 (6)		0.242 (3)	0.467 (24)	nm
BD13	-	-	-	-	1.53 (2)	0.240 (3)	0.382 (4)	1.92 (5)	3.18 (6)
BD14	-	-	-	-	1.15 (2)	0.179 (4)	0.307 (3)	1.23 (4)	nm
BD12b	-	-	-	-	0.413 (6)	0.120 (2)	0.240 (4)	0.490 (24)	nm
McElmo Dome									
Doe Canyon	73.3	19.7	3.94	0.0013	501 (34)	8.08 (8)	33.1 (2)	87.7 (2)	8.55 (15)
MC-1	97.8	1.95	0.13	0.0059	9.58 (8)	0.376 (4)	2.26 (1)	5.99 (8)	9.64 (16)
HE-2	98.2	1.54	0.12	0.0065	70.5 (7)	0.307 (30)	12.1 (1)	22.1 (4)	4.53 (8)
YC-4	97.7	2.00	0.14	0.0065	10.2 (10)	0.573 (6)	2.43 (2)	21.4 (1)	nm
SC-9	97.9	1.82	0.12	0.0064	14.8 (14)	0.497 (5)	2.64 (2)	5.19 (17)	8.48 (14)
YB-2	98.1	1.72	0.12	0.0056	6.42 (61)	0.371 (4)	2.27 (2)	5.07 (13)	11.5 (19)
YC-1	97.7	2.00	0.14	0.0065	12.1 (12)	0.423 (5)	2.40 (2)	5.54 (8)	nm
HF-1	nm	nm	Nm	nm	19.3 (26)	0.564 (12)	4.00 (2)	9.54 (7)	nm
HD-2	97.7	1.98	0.15	0.0068	11.7 (12)	0.128 (2)	2.43 (2)	7.18 (7)	nm
YA-2	98.2	1.53	0.12	0.0073	15.0 (15)	0.130 (2)	2.34 (2)	5.80 (10)	nm
YE-1	98.1	1.63	0.13	0.0071	9.75 (8)	0.143 (3)	2.41 (2)	5.80 (16)	nm
HA-1	97.7	2.00	0.15	0.0061	11.0 (11)	0.205 (7)	2.95 (2)	7.29 (12)	nm
SC-10	98.1	1.64	0.11	0.0059	11.6 (11)	0.413 (5)	2.59 (2)	6.51 (5)	nm
HC-2	98.0	1.72	0.14	0.0068	10.7 (10)	0.409 (5)	2.60 (2)	5.57 (7)	nm
HB-1	97.8	1.91	0.16	0.0077	9.94 (10)	0.247 (4)	2.41 (2)	4.00 (7)	nm
YD-1	97.8	1.94	0.16	0.0072	5.68 (6)	0.366 (5)	2.26 (2)	8.25 (8)	nm
St. John's Dome									
22-1X	82.9	16.0	0.12	0	134 (13)	34.4 (47)	25.9 (2)	641 (10)	nm
10-22	98.9	1.0	0.012	0	9.42 (9)	2.30 (4)	2.52 (2)	67.6 (2)	nm
3-1	91.7	8.0	0.0634	0	70.6 (7)	15.1 (21)	11.7 (1)	290 (9)	nm

1σ errors to last significant figure in brackets, nm=not measured

Table 3: Calculated groundwater noble gas concentrations (cm^3STPcm^{-3}) and ratios

Field & Well McCallum Dome	Observed $^{20}Ne/^{36}Ar$	Proportion ^{36}Ar lost to stage 2 water	Measured ^{36}Ar $cm^3(STP)cm^{-3}$ ($\times 10^{-8}$)	$^{36}Ar_{init}$ $cm^3(STP)cm^{-3}$ ($\times 10^{-8}$)	Stage 1 V_{water}/V_{Gas} (STP)	Stage 2 V_{water}/V_{Gas} (STP)	Stage2 V_{water}/V_{Gas} (RTP)
No. 5	0.462	0.888	2.54	22.6	0.2054	1.487	85.61
No. 36	0.305	0.745	8.91	34.9	0.3169	2.595	49.06
No. 13	0.358	0.815	12.2	65.7	0.5960	2.002	63.59
No. 79	0.312	0.757	8.09	33.3	0.3024	2.418	52.65
Sheep Mtn							
8-2-P	1.209	0.933	1.22	18.2	0.1652	0.967	107.93
2-10-O	2.014	0.973	1.51	56.6	0.5130	1.295	144.56
9-26	0.645	0.792	0.950	4.58	0.0415	0.562	62.77
2-9-H	3.076	0.988	3.18	255	2.3173	1.570	175.20
3-15-B	0.843	0.872	1.83	14.3	0.1294	0.734	81.88
4-13	0.927	0.892	1.20	11.1	0.1010	0.796	88.85
4-26-E	0.530	0.704	0.835	2.82	0.0256	0.436	48.61
3-23-D	0.535	0.710	1.08	3.72	0.0338	0.442	49.36
7-35-L	0.922	0.891	0.812	7.45	0.0676	0.792	88.43
2-35-C	0.675	0.809	0.849	4.44	0.0403	0.591	65.96
1-15-C	2.263	0.978	0.299	138	1.2555	1.372	153.09
3-4-O	0.762	0.846	0.346	22.5	0.2040	0.669	74.70
4-14-M	1.216	0.934	0.911	13.8	0.1249	0.971	108.35
5-15-O	2.496	0.982	0.173	95.7	0.8678	1.435	160.11
4-4-P	1.311	0.942	0.998	17.3	0.1566	1.019	113.76
5-9-A	1.104	0.921	1.16	14.7	0.1332	0.907	101.27
1-1-J	0.635	0.787	1.38	6.48	0.0588	0.552	61.66
1-22-H	0.658	0.800	1.42	7.11	0.0645	0.575	64.21
Bravo Dome							
BD01	0.362	0.786	0.212	0.992	0.0090	1.261	87.01
BD02	0.426	0.841	1.25	7.87	0.0714	1.502	103.60
BD03	0.430	0.843	0.881	5.62	0.0510	1.513	104.39
BD04	0.406	0.826	0.222	1.27	0.0115	1.429	98.57
BD05	0.385	0.809	0.873	4.56	0.0414	1.351	93.24
BD06	0.349	0.772	0.299	1.31	0.0119	1.206	83.23
BD07	0.279	0.661	0.191	0.562	0.0051	0.883	60.95
BD08	0.314	0.726	0.505	1.84	0.0167	1.057	72.94
BD09							0.00
BD10	0.395	0.818	0.499	2.73	0.0248	1.389	95.83
BD11	0.152	0.00	0.0549	0.0547	0.0005		0.00
BD12							0.00
BD13	0.347	0.770	0.406	1.76	0.0160	1.199	82.73
BD14	0.296	0.695	0.290	0.948	0.0086	0.969	66.86
BD12b	0.430	0.843	0.0494	0.315	0.0029	1.513	104.39
McElmo Dome							
Doe Canyon	0.197	0.427	41.1	71.7	0.6505	0.132	24.81
MC-1	0.257	0.678	1.46	4.55	0.0413	0.268	50.42
HE-2	0.354	0.840	8.66	54.1	0.4912	0.434	81.53
YC-4	0.061	0.000	9.34	9.34	0.0847		0.00
SC-9	0.307	0.783	1.62	7.44	0.0674	0.361	67.82
YB-2	0.253	0.669	1.47	4.42	0.0401	0.262	49.18
YC-1	0.267	0.704	1.58	5.36	0.0486	0.288	54.16
HF-1	0.198	0.430	2.85	5.00	0.0453	0.133	25.01
HD-2	0.106	0.000	1.20	1.20	0.0109		0.00
YA-2	0.103	0.000	1.27	1.27	0.0115		0.00
YE-1	0.110	0.000	1.30	1.30	0.0118		0.00
HA-1	0.128	0.000	1.59	1.59	0.0145		0.00
SC-10	0.338	0.823	1.22	6.91	0.0627	0.409	76.95
HC-2	0.389	0.870	1.05	8.07	0.0732	0.482	90.56
HB-1	0.228	0.584	1.08	2.61	0.0236	0.207	38.96
YD-1	0.319	0.799	1.15	5.73	0.0520	0.380	71.43
St. John's Dome							
22-1X	0.182	0.320	189	278	2.5251	0.289	14.89
10-22	0.136	0.000	16.9	16.9	0.1534		0.00
3-1	0.219	0.544	69.2	152	1.3784	0.592	30.53

Table 4: Reservoir Conditions Used in Models

Reservoir	Average Depth (m)	Pressure (MPa)	Bore Hole Temp (K)	TDS (mg/l)	KNe (GPa)	KAr (GPa)	KKr (GPa)	KXe (GPa)
Bravo Dome[a]	820	8.03	314	85000	18.57	8.16	5.49	3.80
McCallum Dome[c]	1630	15.97	333	13300	13.33	6.56	4.86	3.28
McElmo Dome[b]	2450	24.00	344	20000	13.08	7.06	5.48	3.79
Sheep Mountain[c]	1400	13.71	331	800	12.79	6.10	4.43	3.05
St. Johns Dome[b]	630	6.17	322	4210	13.35	5.78	3.82	2.71

[a] Broadhead (1993)
[b] Stevens et al., (2004)
[c] Field Operators

Figure captions for appendix

Fig. A1. Top surface map of the Tubb sandstone at Bravo Dome showing the folded and faulted structure of the field. Also shown is the approximate location of the gas/water contact which is poorly defined to the southwest. Contours are in feet above Mean Sea Level (MSL). Figure modified from Cassidy, (2006).

Fig. A2. Structure map of the top Dakota Formation illustrating the well locations sampled for this study and the complex folded and thrusted reservoir geology. Contours are in feet above MSL. The gas water contact is located at approximately 4000 feet across the reservoir. Figure modified from Roth (1983).

Fig. A3. Top surface map of the Leadville limestone at McElmo Dome showing the faulted complex structure of the field, approximate position of the gas/water contact and the wide distribution of wells sampled in this study. Contours are in feet below mean sea level. (Modified from Stevens, 2004).

Fig. A4. Top surface map of Permian Supai formation at St. John's Dome showing the faulted anticlinal structure of the field and the position of the three wells sampled in this study. Contours are in feet above mean sea level. (Modified from Rauzi, 1999 by Reddy).

Figure 1

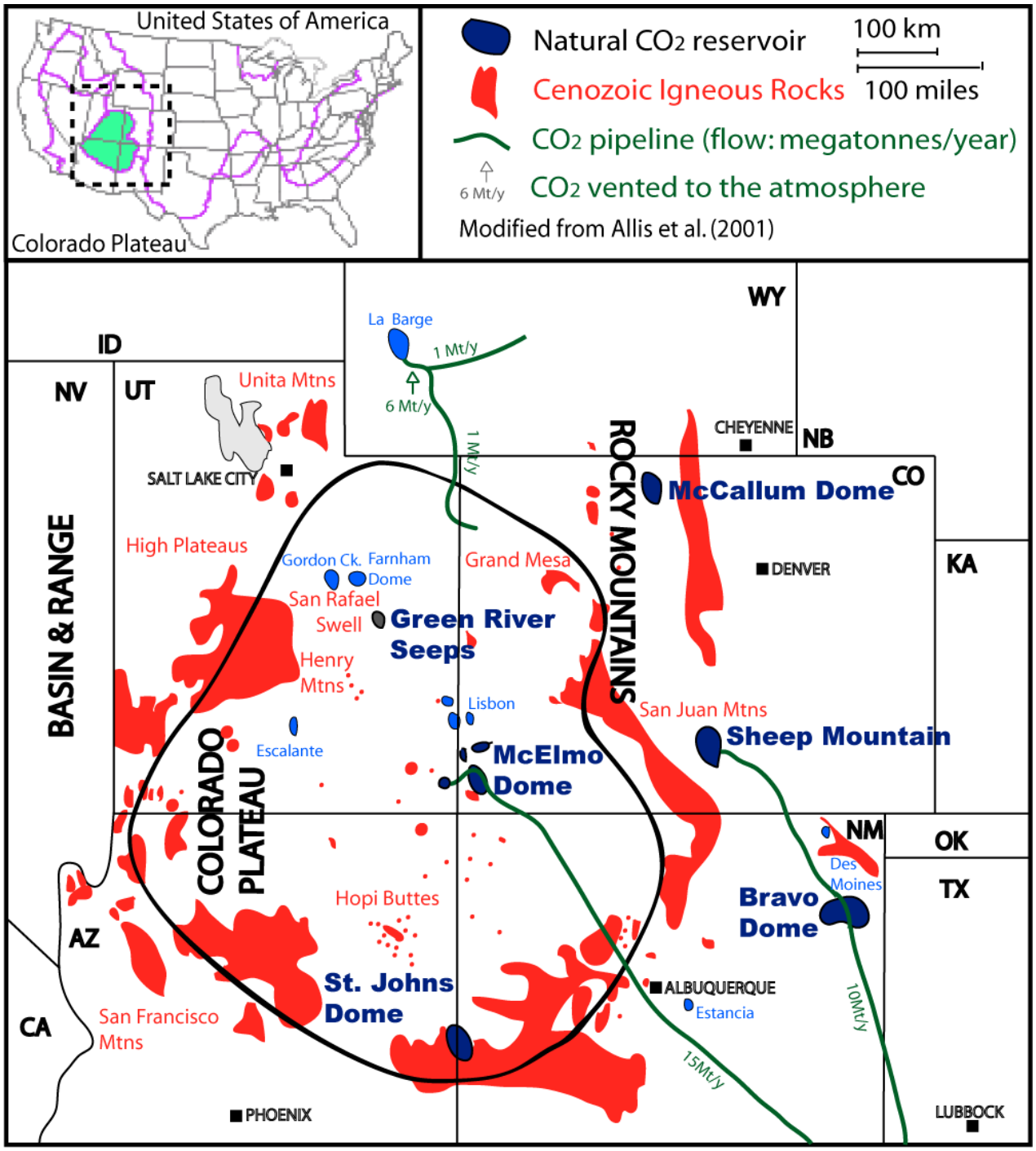
United States of America
Colorado Plateau
Natural CO2 reservoir
100 km
100 miles
Cenozoic Igneous Rocks
CO2 pipeline (flow: megatonnes/year)
6 Mt/y
CO2 vented to the atmosphere
Modified from Allis et al. (2001)
WY
ID
NV
UT
La Barge
1 Mt/y
6 Mt/y
Unita Mtns
SALT LAKE CITY
CHEYENNE
NB
CO
McCallum Dome
ROCKY MOUNTAINS
BASIN & RANGE
High Plateaus
Gordon Ck.
Farnham Dome
Grand Mesa
DENVER
KA
San Rafael Swell
Green River Seeps
Henry Mtns
Lisbon
San Juan Mtns
Sheep Mountain
Escalante
McElmo Dome
COLORADO PLATEAU
NM
OK
TX
Des Moines
Hopi Buttes
Bravo Dome
AZ
St. Johns Dome
ALBUQUERQUE
Estancia
10Mt/y
15Mt/y
CA
San Francisco Mtns
PHOENIX
LUBBOCK

Figure 2

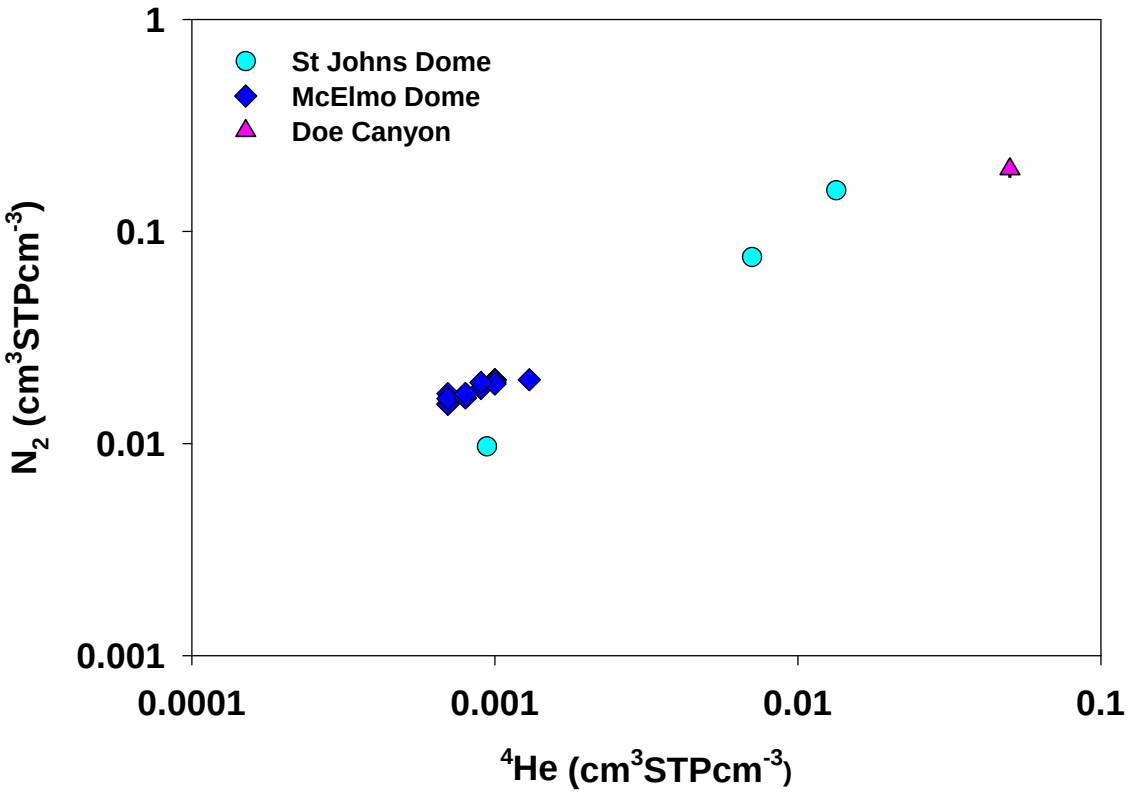
St Johns Dome
McElmo Dome
Doe Canyon
1
0.1
0.01
0.001
0.0001
0.001
0.01
0.1
N2 (cm3STPcm-3)
4He (cm3STPcm-3)

Figure 3

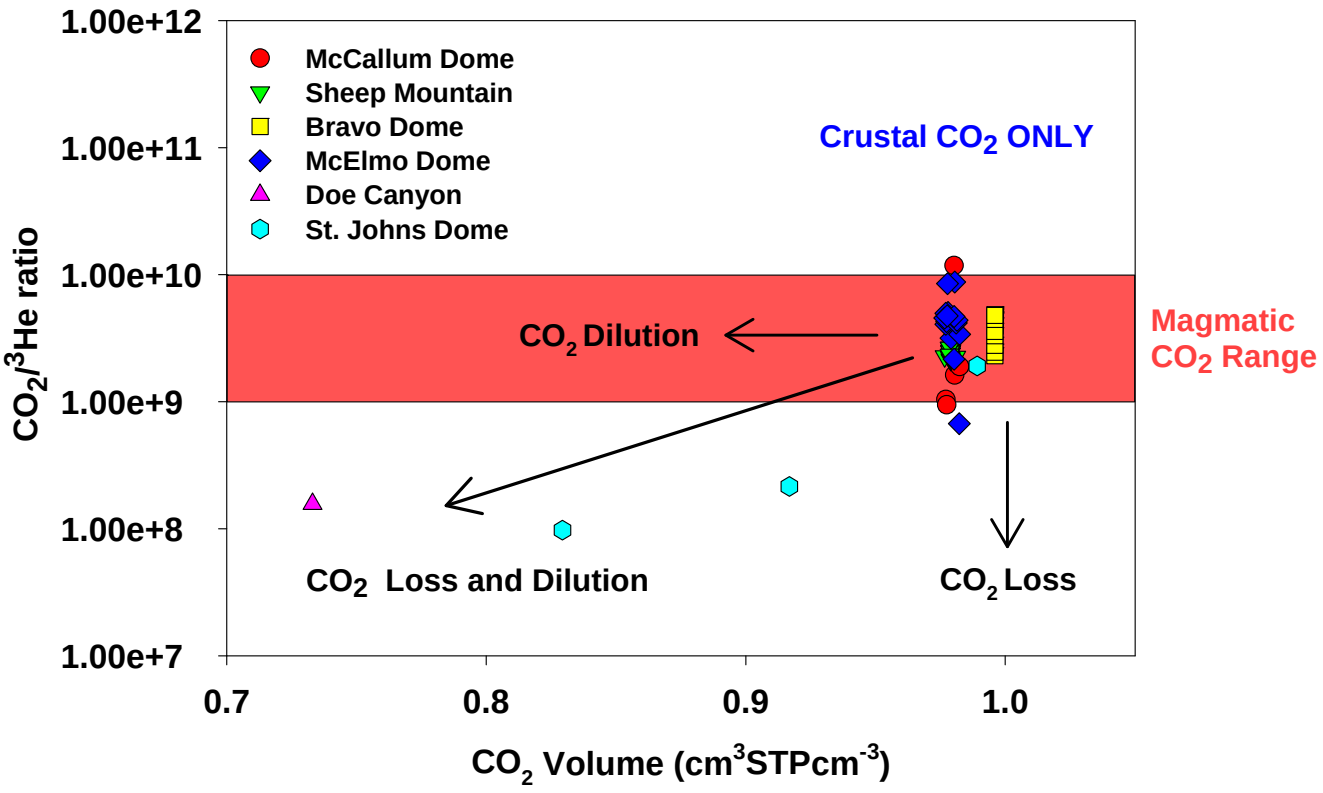
1.00e+12
1.00e+11
1.00e+10
1.00e+9
1.00e+8
1.00e+7
$CO_2/^3He$ ratio
McCallum Dome
Sheep Mountain
Bravo Dome
McElmo Dome
Doe Canyon
St. Johns Dome
Crustal CO_2 ONLY
CO_2 Dilution
Magmatic CO_2 Range
CO_2 Loss and Dilution
CO_2 Loss
0.7
0.8
0.9
1.0
CO_2 Volume (cm^3STPcm^{-3})

Figure 4

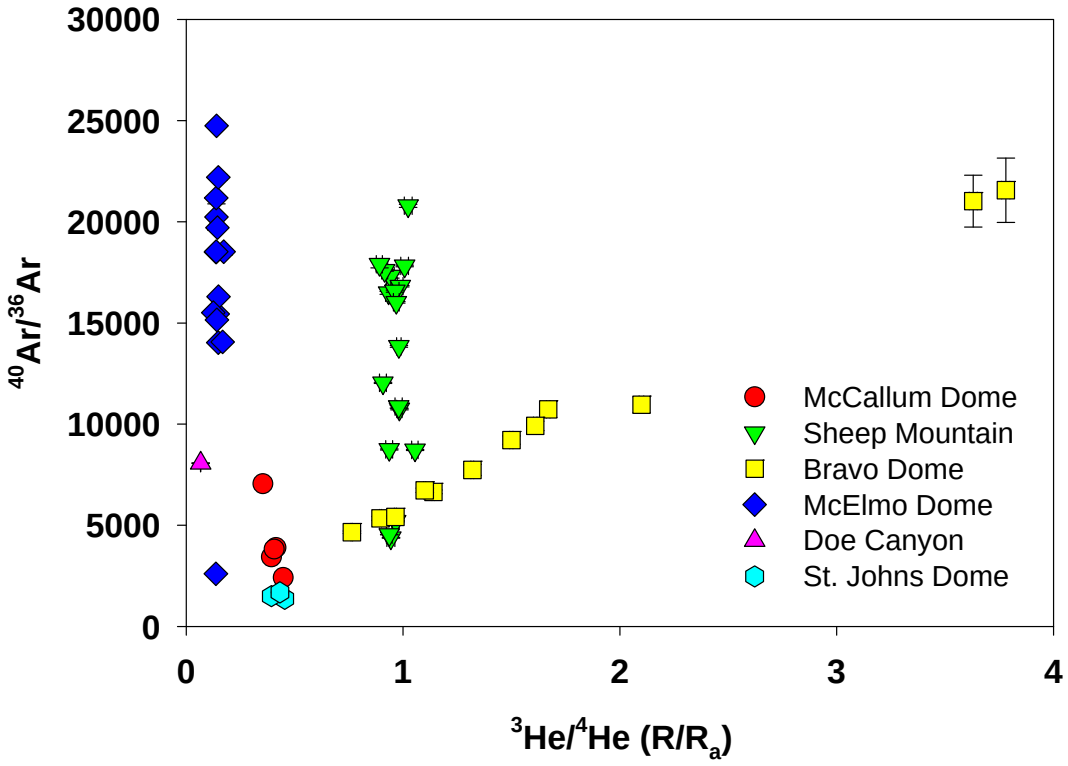
30000
25000
20000
15000
10000
5000
0
$^{40}Ar/^{36}Ar$
0
1
2
3
4
$^{3}He/^{4}He$ (R/R_a)
McCallum Dome
Sheep Mountain
Bravo Dome
McElmo Dome
Doe Canyon
St. Johns Dome

Figure 5

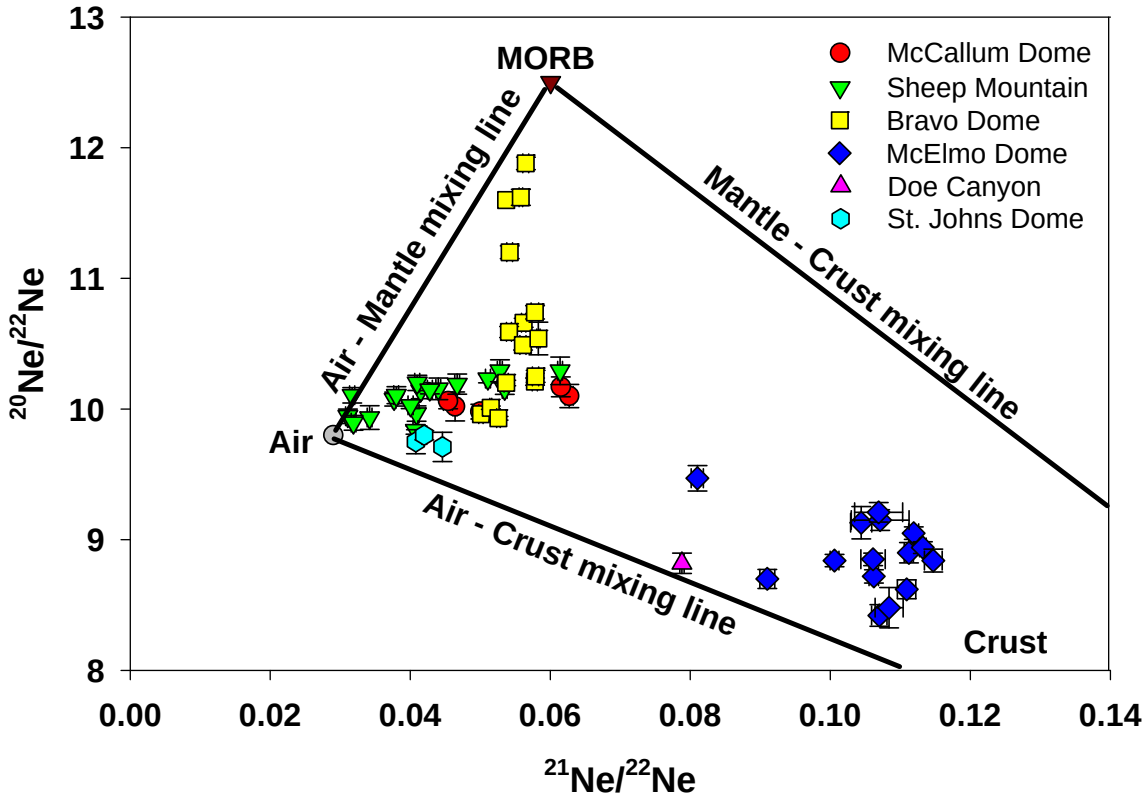
MORB
Air
Crust
Air - Mantle mixing line
Mantle - Crust mixing line
Air - Crust mixing line
McCallum Dome
Sheep Mountain
Bravo Dome
McElmo Dome
Doe Canyon
St. Johns Dome
20Ne/22Ne
21Ne/22Ne
13
12
11
10
9
8
0.00
0.02
0.04
0.06
0.08
0.10
0.12
0.14

Figure 6a

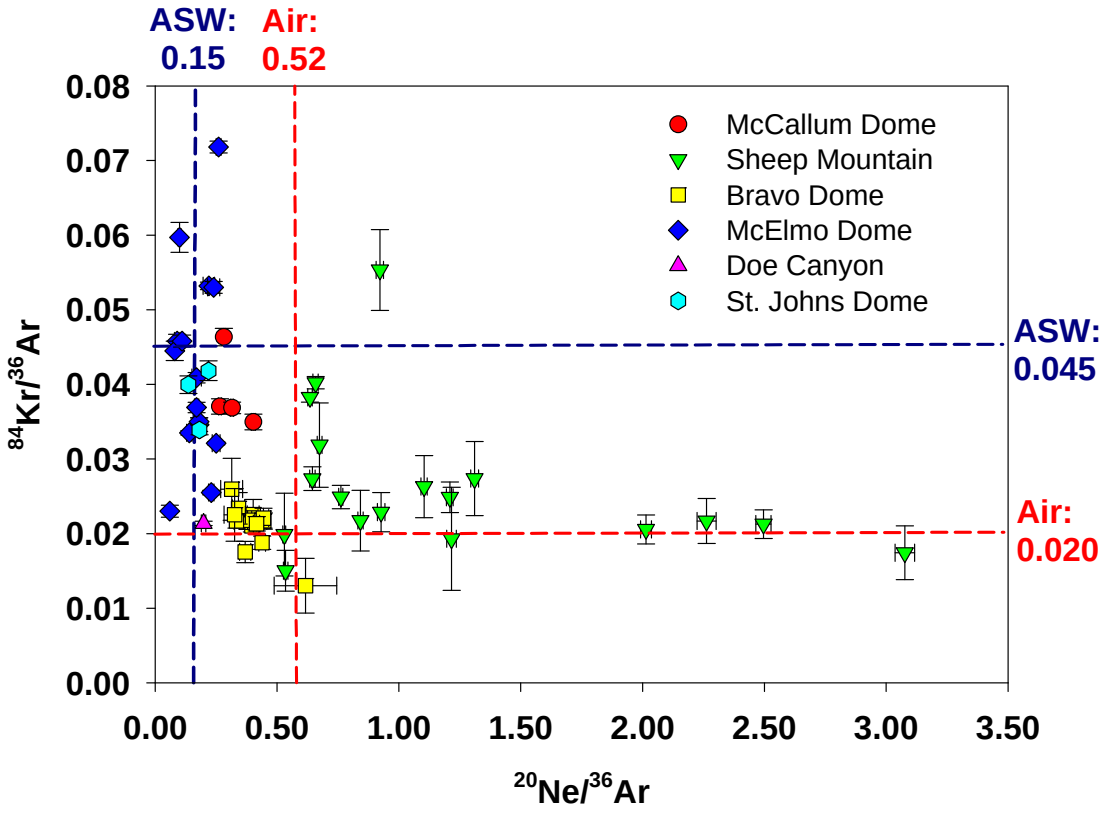
ASW:
0.15
Air:
0.52
McCallum Dome
Sheep Mountain
Bravo Dome
McElmo Dome
Doe Canyon
St. Johns Dome
ASW:
0.045
Air:
0.020
84Kr/36Ar
20Ne/36Ar
0.00
0.01
0.02
0.03
0.04
0.05
0.06
0.07
0.08
0.00
0.50
1.00
1.50
2.00
2.50
3.00
3.50

Figure 6b

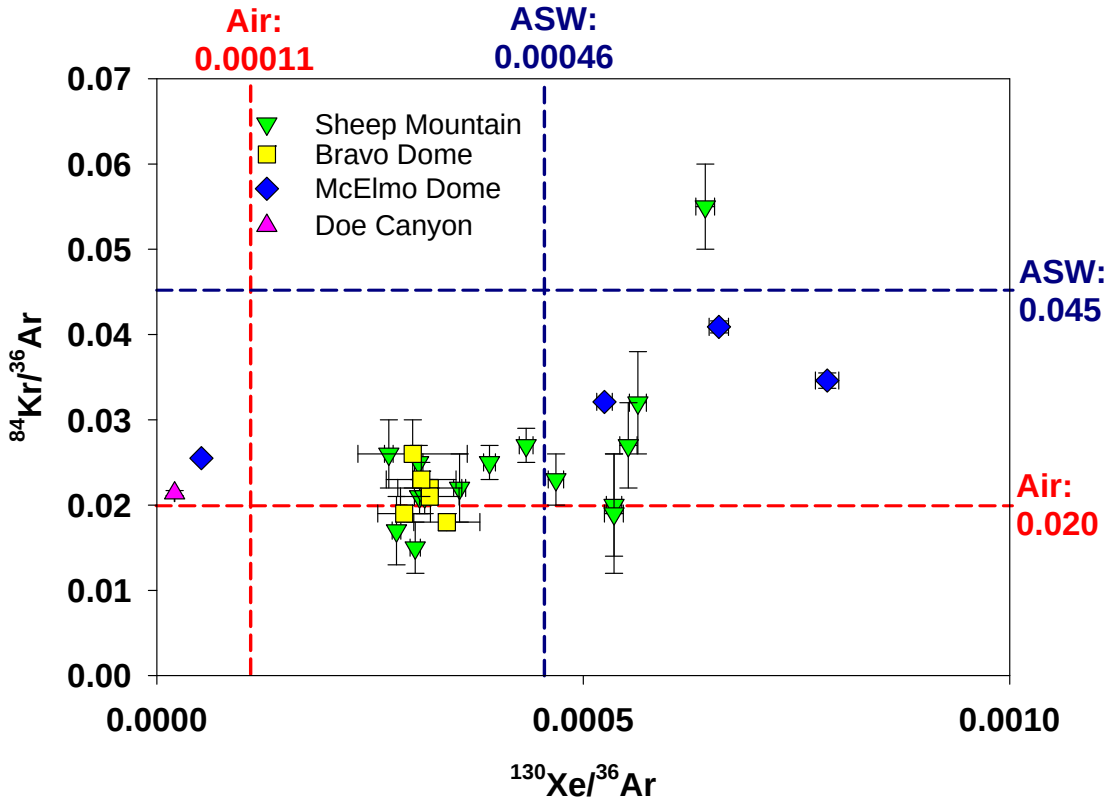
Air:
0.00011
ASW:
0.00046
Sheep Mountain
Bravo Dome
McElmo Dome
Doe Canyon
ASW:
0.045
Air:
0.020
0.07
0.06
0.05
0.04
0.03
0.02
0.01
0.00
0.0000
0.0005
0.0010
84Kr/36Ar
130Xe/36Ar

Figure 7

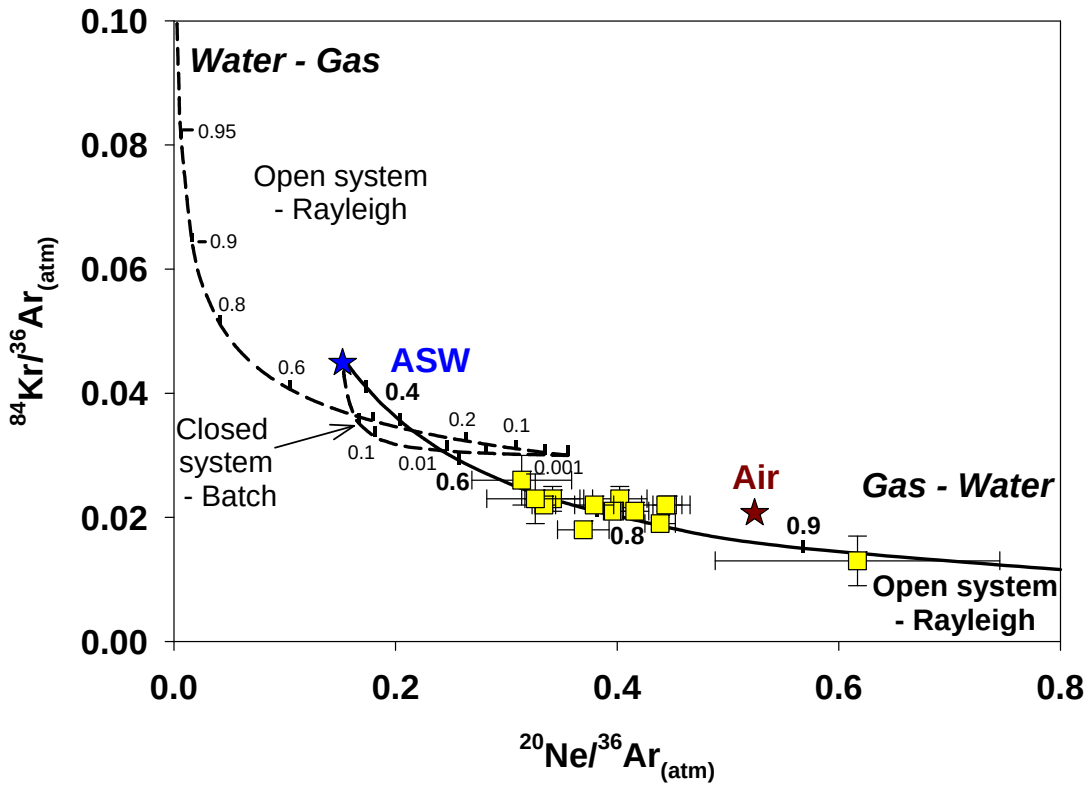
Water - Gas
0.95
0.9
0.8
0.6
Open system
- Rayleigh
ASW
0.4
0.2
0.1
Closed
system
- Batch
0.1
0.01
0.001
0.6
Air
0.9
0.8
Gas - Water
Open system
- Rayleigh
0.10
0.08
0.06
0.04
0.02
0.00
0.0
0.2
0.4
0.6
0.8
84Kr/36Ar(atm)
20Ne/36Ar(atm)

Figure 8

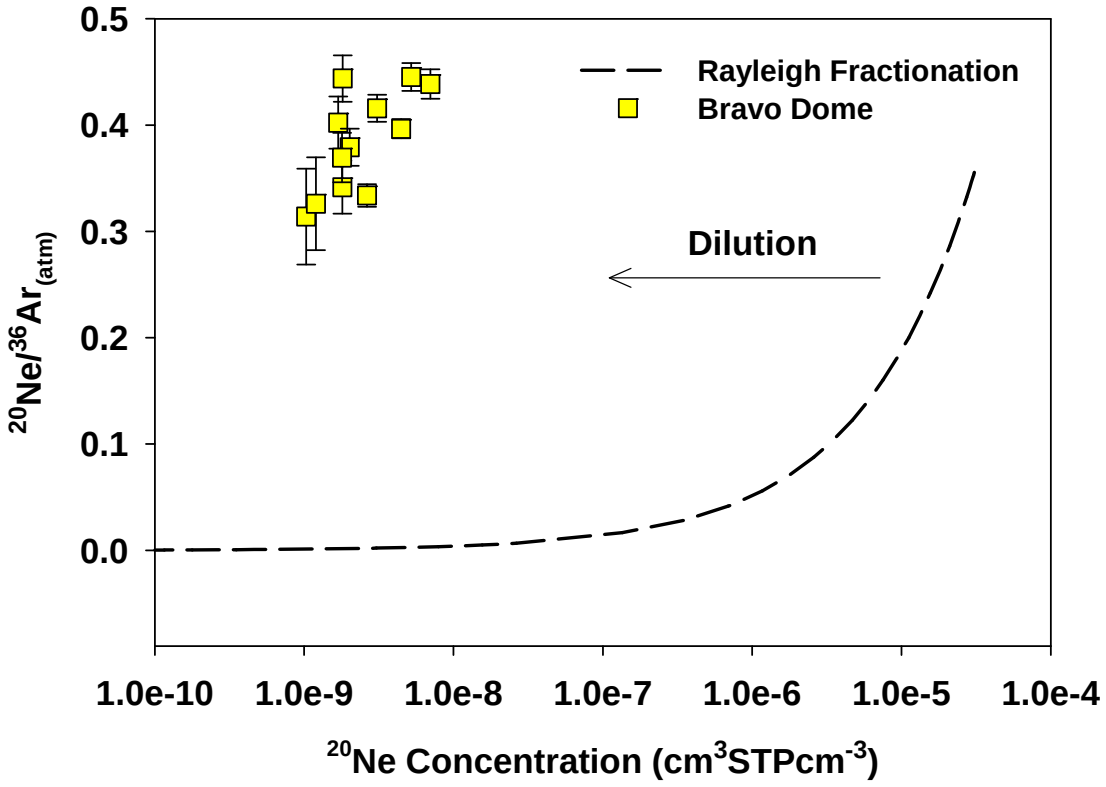
0.5
0.4
0.3
0.2
0.1
0.0
$^{20}Ne/^{36}Ar_{(atm)}$
Rayleigh Fractionation
Bravo Dome
Dilution
1.0e-10
1.0e-9
1.0e-8
1.0e-7
1.0e-6
1.0e-5
1.0e-4
^{20}Ne Concentration (cm^3STPcm^{-3})

Figure 9

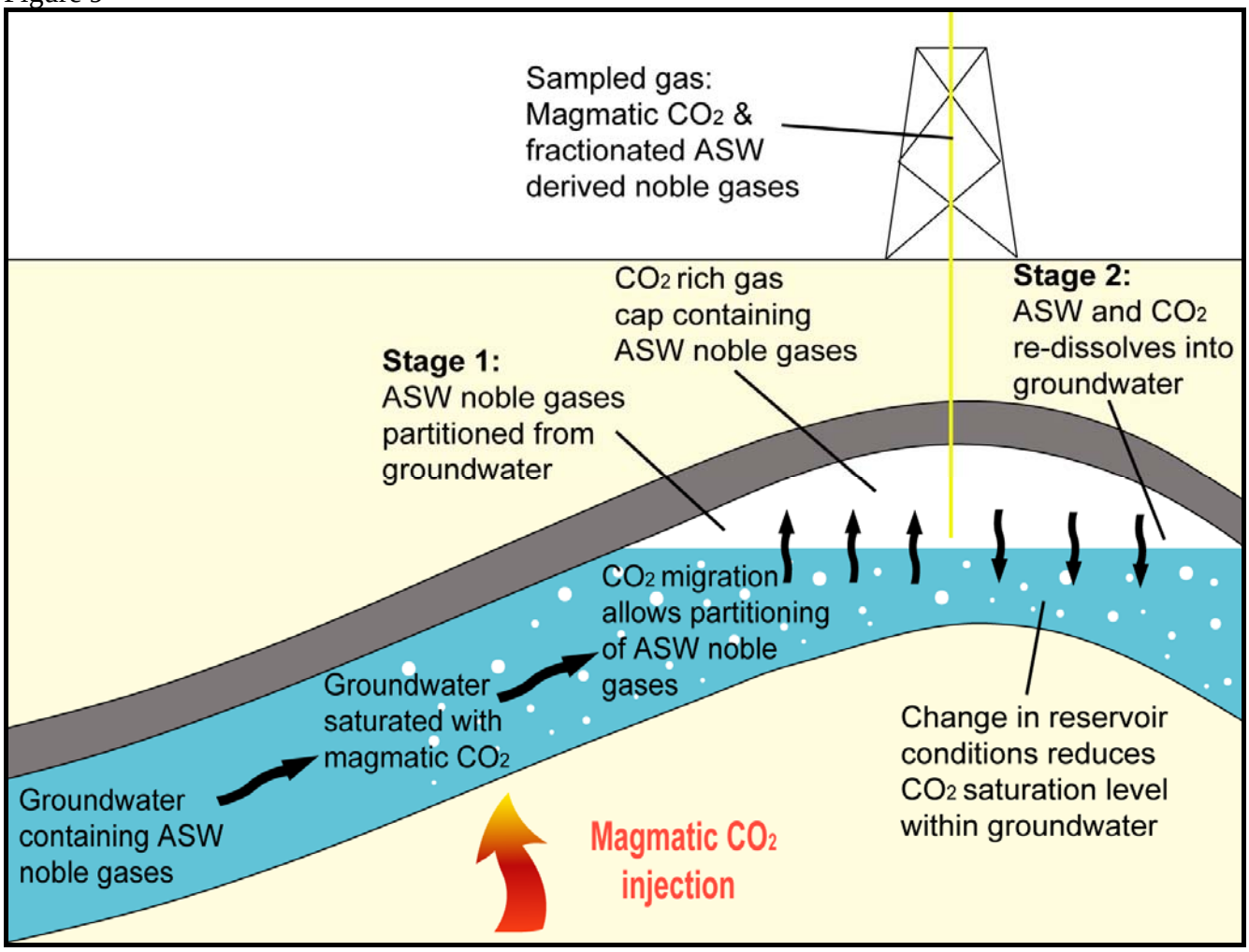
Sampled gas:
Magmatic CO2 &
fractionated ASW
derived noble gases
CO2 rich gas
cap containing
ASW noble gases
Stage 2:
ASW and CO2
re-dissolves into
groundwater
Stage 1:
ASW noble gases
partitioned from
groundwater
CO2 migration
allows partitioning
of ASW noble
gases
Groundwater
saturated with
magmatic CO2
Groundwater
containing ASW
noble gases
Change in reservoir
conditions reduces
CO2 saturation level
within groundwater
Magmatic CO2
injection

Figure 10a

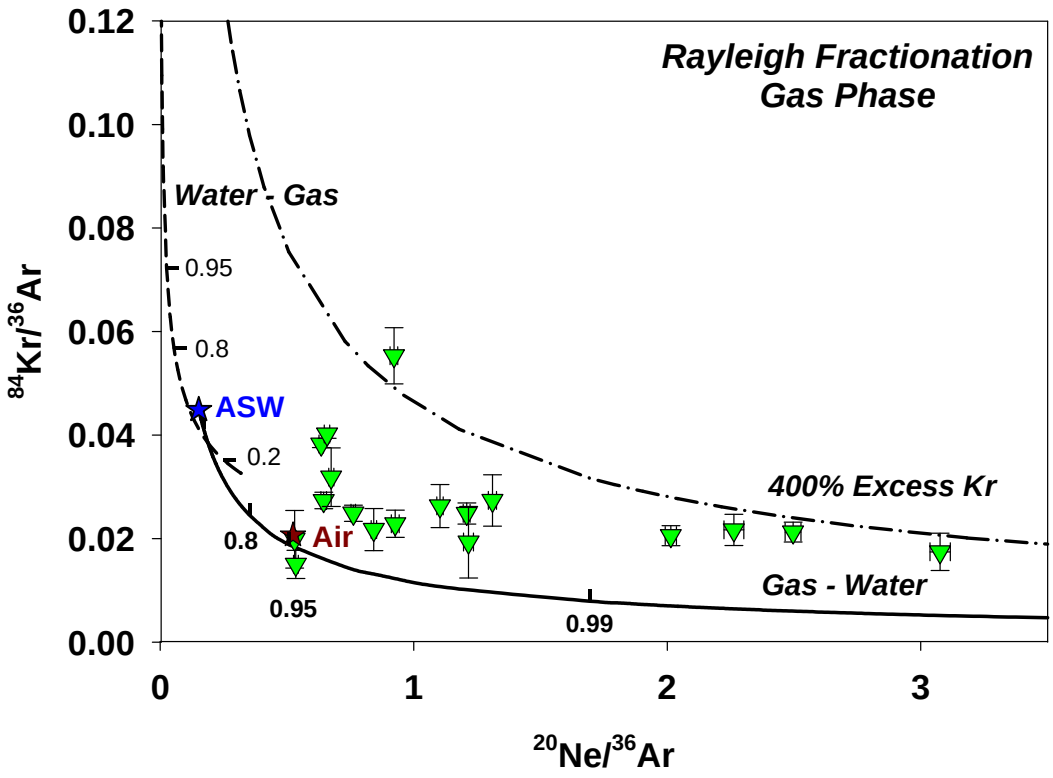
Rayleigh Fractionation
Gas Phase
Water - Gas
0.95
0.8
ASW
0.2
0.8
Air
0.95
0.99
400% Excess Kr
Gas - Water
0.12
0.10
0.08
0.06
0.04
0.02
0.00
0
1
2
3
84Kr/36Ar
20Ne/36Ar

Figure 10b

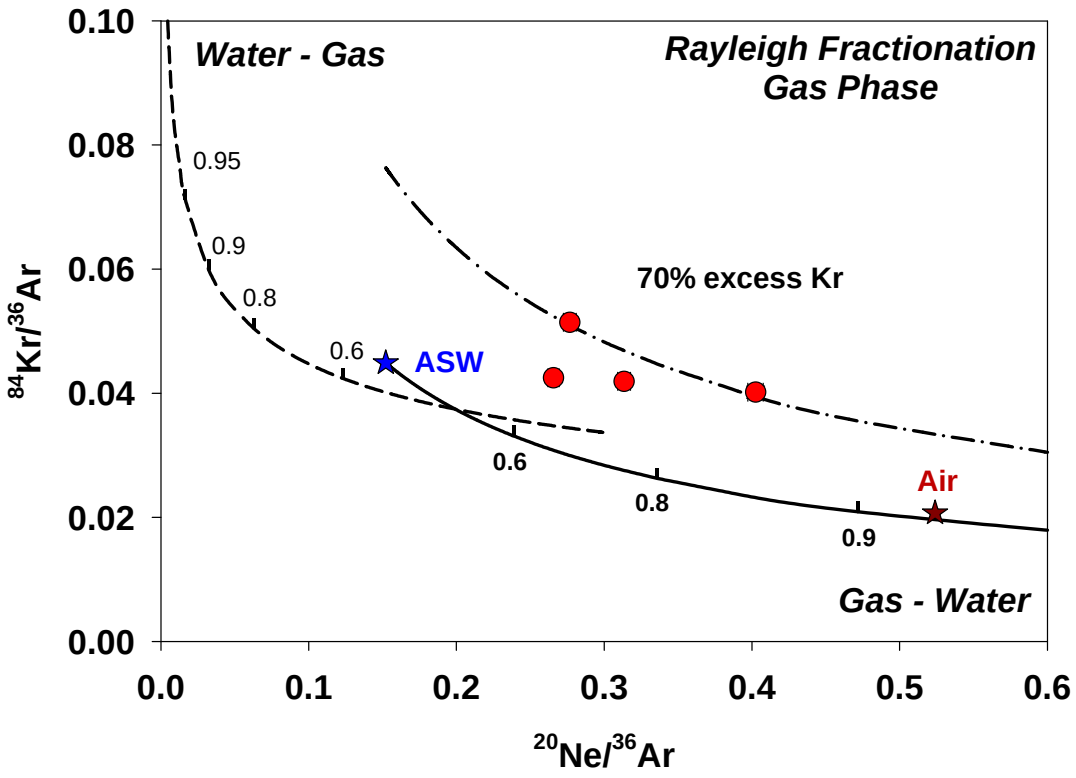
Water - Gas
Rayleigh Fractionation
Gas Phase
0.95
0.9
0.8
0.6
ASW
70% excess Kr
0.6
0.8
0.9
Air
Gas - Water
0.10
0.08
0.06
0.04
0.02
0.00
0.0
0.1
0.2
0.3
0.4
0.5
0.6
84Kr/36Ar
20Ne/36Ar

Figure A1

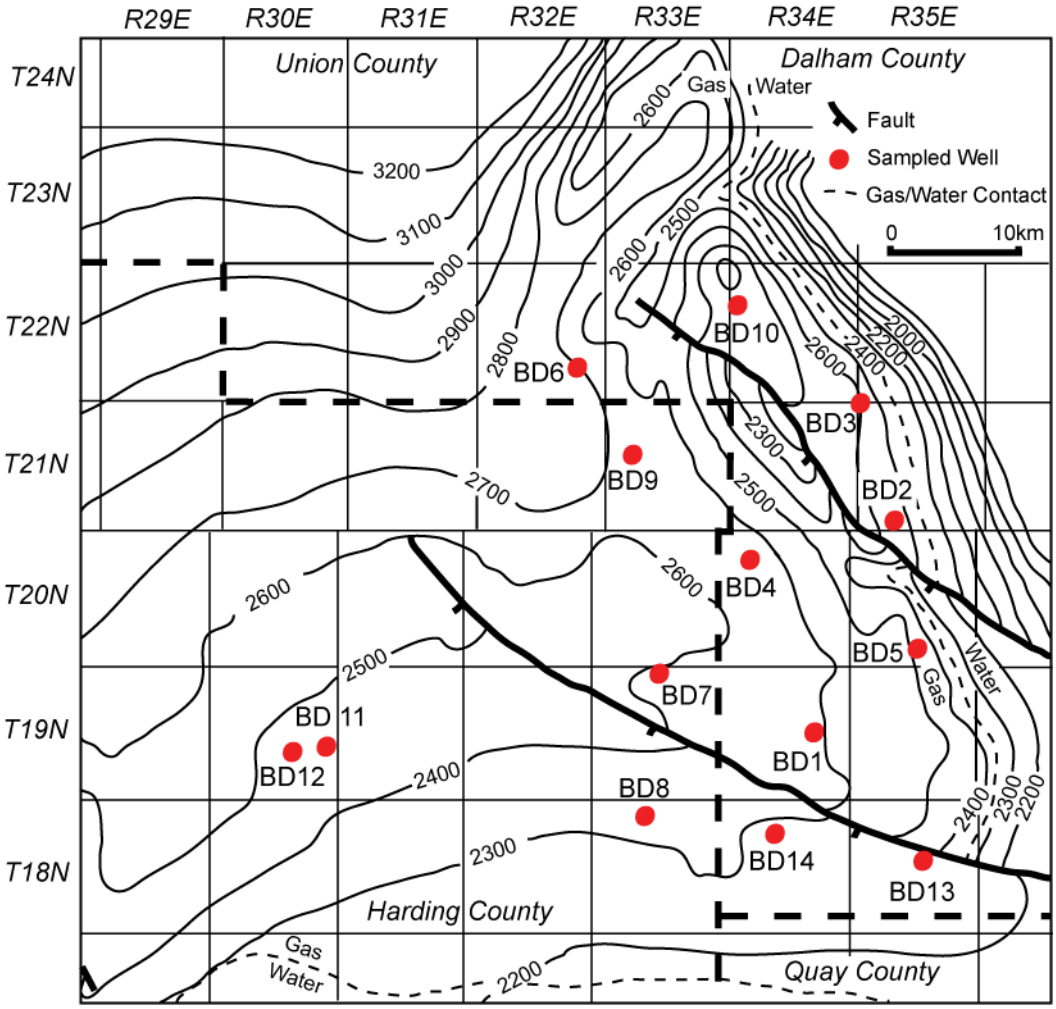
R29E
R30E
R31E
R32E
R33E
R34E
R35E
T24N
T23N
T22N
T21N
T20N
T19N
T18N
Union County
Dalham County
Harding County
Quay County
Gas
Water
Fault
Sampled Well
Gas/Water Contact
0
10km
BD1
BD2
BD3
BD4
BD5
BD6
BD7
BD8
BD9
BD10
BD11
BD12
BD13
BD14
2000
2200
2300
2400
2500
2600
2700
2800
2900
3000
3100
3200

Figure A2

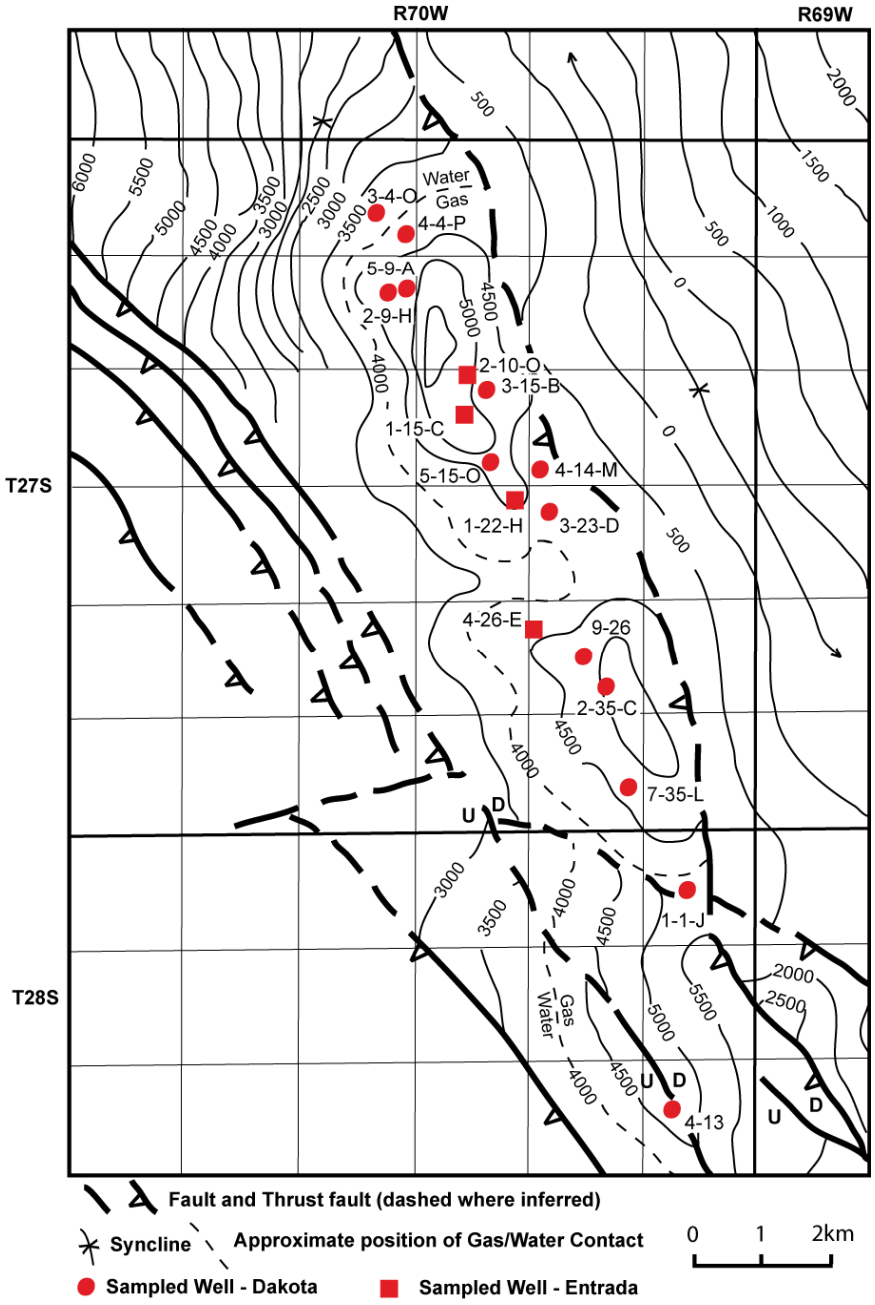
R70W
R69W
T27S
T28S
3-4-O
Water
Gas
4-4-P
5-9-A
2-9-H
2-10-O
3-15-B
1-15-C
5-15-O
4-14-M
1-22-H
3-23-D
4-26-E
9-26
2-35-C
7-35-L
1-1-J
4-13
U
D
Fault and Thrust fault (dashed where inferred)
Syncline
Approximate position of Gas/Water Contact
Sampled Well - Dakota
Sampled Well - Entrada
0
1
2km

Figure A3

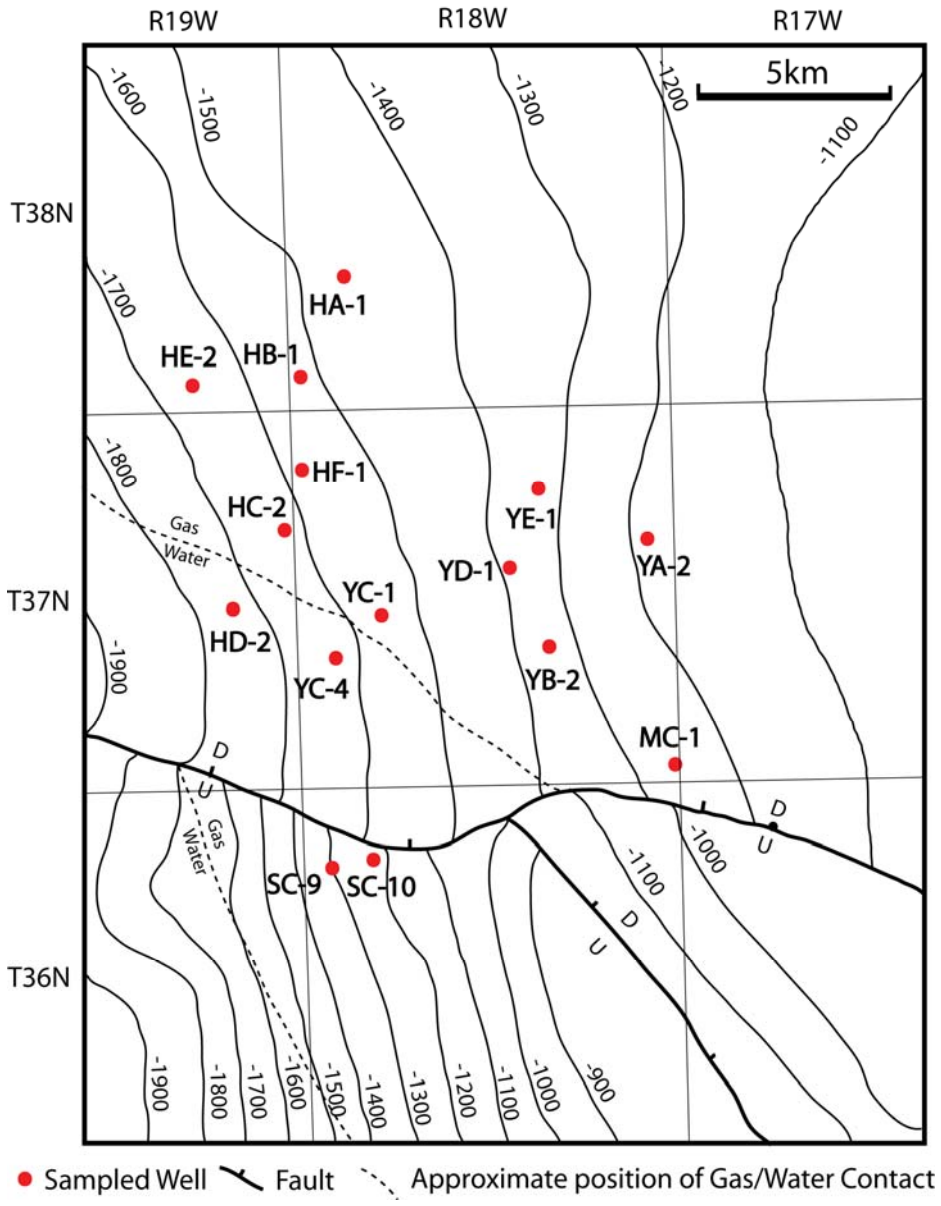
R19W
R18W
R17W
5km
T38N
T37N
T36N
-1600
-1500
-1400
-1300
-1200
-1100
-1700
-1800
-1900
-1000
-900
HA-1
HE-2
HB-1
HF-1
HC-2
YE-1
YD-1
YA-2
YC-1
HD-2
YC-4
YB-2
MC-1
SC-9
SC-10
Gas
Water
D
U
Sampled Well
Fault
Approximate position of Gas/Water Contact

Figure A4

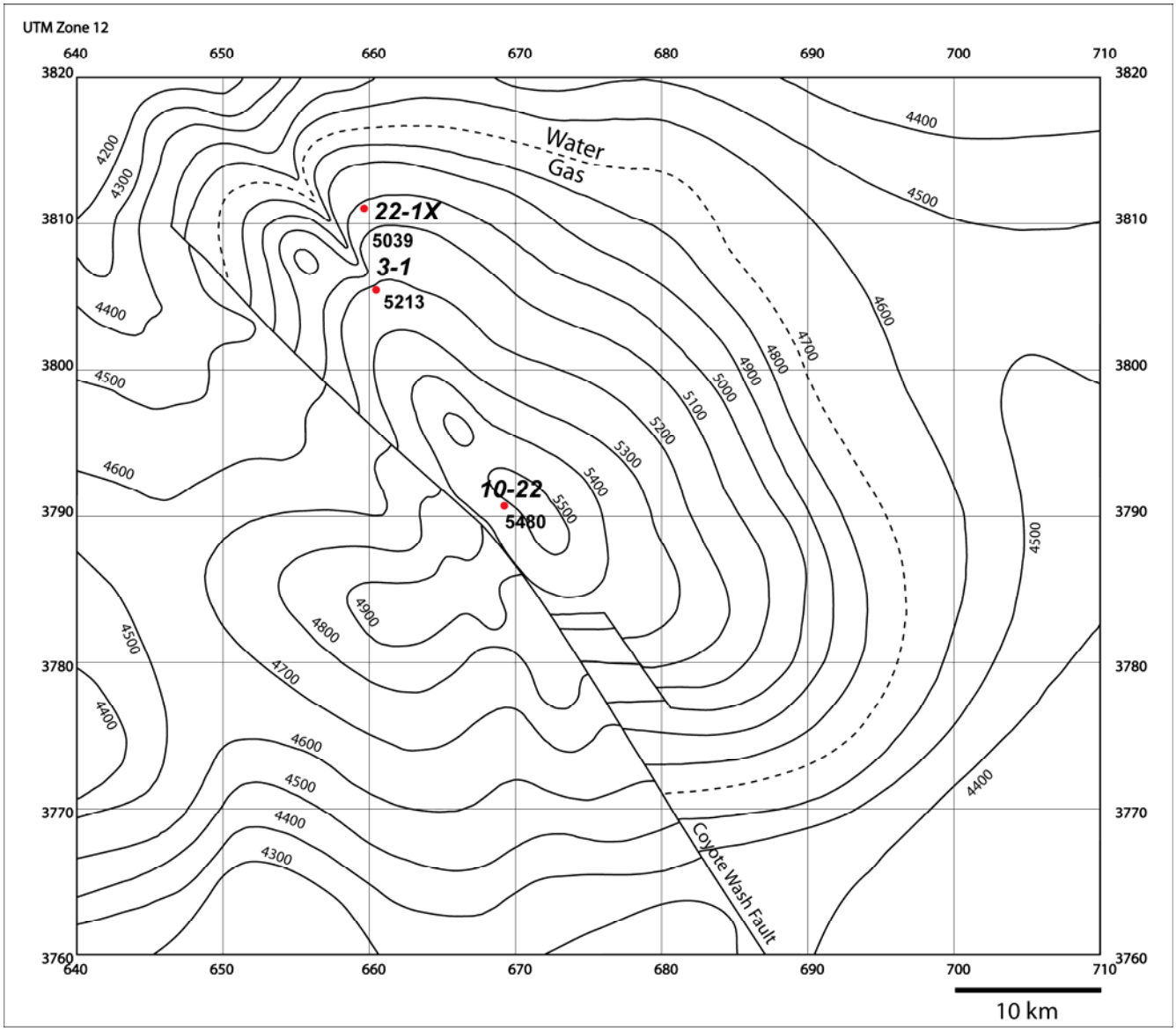
UTM Zone 12
640
650
660
670
680
690
700
710
3820
3810
3800
3790
3780
3770
3760
Water
Gas
22-1X
5039
3-1
5213
10-22
5480
Coyote Wash Fault
10 km